Biophysical *Journal*
Article

Biophysical Society

Gramicidin Increases Lipid Flip-Flop in Symmetric and Asymmetric Lipid Vesicles

Milka Doktorova,[1,*] Frederick A. Heberle,[2,3] Drew Marquardt,[4] Radda Rusinova,[5] R. Lea Sanford,[5] Thasin A. Peyear,[5] John Katsaras,[6,7] Gerald W. Feigenson,[8] Harel Weinstein,[5,9] and Olaf S. Andersen[5]

[1]Tri-Institutional PhD Program in Computational Biology and Medicine, Weill Cornell Medical College, New York, New York; [2]Department of Integrative Biology and Pharmacology, University of Texas Health Science Center, Houston, Texas; [3]The Bredesen Center for Interdisciplinary Research and Graduate Education, University of Tennessee, Knoxville, Tennessee; [4]University of Windsor, Ontario, Canada; [5]Department of Physiology and Biophysics, Weill Cornell Medical College, New York, New York; [6]Large Scale Structures Group, Oak Ridge National Laboratory, Oak Ridge, Tennessee and [7]Shull Wollan Center, Oak Ridge National Laboratory, Oak Ridge, Tennessee; [8]Department of Molecular Biology and Genetics, Cornell University, Ithaca, New York; and [9]The HRH Prince Alwaleed Bin Talal Bin Abdulaziz Alsaud Institute for Computational Biomedicine, Weill Greenberg Center, New York, New York

ABSTRACT Unlike most transmembrane proteins, phospholipids can migrate from one leaflet of the membrane to the other. Because this spontaneous lipid translocation (flip-flop) tends to be very slow, cells facilitate the process with enzymes that catalyze the transmembrane movement and thereby regulate the transbilayer lipid distribution. Nonenzymatic membrane-spanning proteins with unrelated primary functions have also been found to accelerate lipid flip-flop in a nonspecific manner and by various hypothesized mechanisms. Using deuterated phospholipids, we examined the acceleration of flip-flop by gramicidin channels, which have well-defined structures and known functions, features that make them ideal candidates for probing the protein-membrane interactions underlying lipid flip-flop. To study compositionally and isotopically asymmetric proteoliposomes containing gramicidin, we expanded a recently developed protocol for the preparation and characterization of lipid-only asymmetric vesicles. Channel incorporation, conformation, and function were examined with small angle x-ray scattering, circular dichroism, and a stopped-flow spectrofluorometric assay, respectively. As a measure of lipid scrambling, we used differential scanning calorimetry to monitor the effect of gramicidin on the melting transition temperatures of the two bilayer leaflets. The two calorimetric peaks of the individual leaflets merged into a single peak over time, suggestive of scrambling, and the effect of the channel on the transbilayer lipid distribution in both symmetric 1-palmitoyl-2-oleoyl-*sn*-glycero-3-phosphocholine and asymmetric 1-palmitoyl-2-oleoyl-*sn*-glycero-3-phosphocholine/1,2-dimyristoyl-*sn*-glycero-3-phosphocholine vesicles was quantified from proton NMR measurements. Our results show that gramicidin increases lipid flip-flop in a complex, concentration-dependent manner. To determine the molecular mechanism of the process, we used molecular dynamics simulations and further computational analysis of the trajectories to estimate the extent of membrane deformation. Together, the experimental and computational approaches were found to constitute an effective means for studying the effects of transmembrane proteins on lipid distribution in both symmetric and asymmetric model membranes.

INTRODUCTION

Membranes are an essential component of all living organisms. Their structure and organization serve many functions and are tightly regulated by the cell. One prominent example is the transverse lipid distribution in cell membranes; whereas a self-assembled lipid bilayer will have the same lipid composition in its two leaflets (i.e., it is symmetric), the leaflet compositions in the plasma membranes of eukaryotic cells differ (i.e., the bilayer is asymmetric), and this difference is actively maintained by the cell. Not surprisingly, the biophysical mechanisms underlying membrane asymmetry are the subject of intense studies (1–5), which are rapidly increasing in number as a result of recent advances that enable the preparation and biophysical characterization of asymmetric lipid-only model membranes in vitro (6–8). Because such model membranes are not at chemical equilibrium and their asymmetry is not actively maintained, the time window for examining their properties is limited by the gradual redistribution of the lipids between the two leaflets until a symmetric lipid composition is achieved. Such unassisted interleaflet lipid movement is often referred to as passive or spontaneous lipid flip-flop (9).

Submitted August 2, 2018, and accepted for publication January 9, 2019.

*Correspondence: milka.n.doktorova@uth.tmc.edu

Milka Doktorova's present address is Department of Integrative Biology and Pharmacology, University of Texas Health Science Center, Houston, Texas.

Editor: Charles Deber.

https://doi.org/10.1016/j.bpj.2019.01.016

Some of the key lipid and bilayer properties that determine the kinetics of spontaneous lipid flip-flop include chain length, headgroup size and charge, and cholesterol concentration, although the mechanism(s) are not fully understood (see (10) for a recent review of both experimental and computational studies on the topic). In general, flip-flop of phospholipids is many orders of magnitude slower than other lipid motions, such as rotation or lateral diffusion (11). This difference is due to the large energy barrier for moving a polar lipid headgroup from one side of the bilayer to the other, a process that requires traversing the bilayer's hydrophobic core. In cells, the one-directional movement of lipids between the two leaflets is catalyzed by ATP-dependent enzymes; these include flippases that move phospholipids from the extracellular leaflet to the intracellular leaflet (e.g., P-type ATPases) (12) and floppases that move phospholipids in the opposite direction (e.g., ATP-binding cassette transporters) (13). An additional bidirectional and often nonspecific movement of lipids across the two leaflets is catalyzed by ATP-independent scramblases, which include the Ca^{2+}-activated TMEM family of proteins (11). It is through a careful balance between the activity of the enzymes and scramblases that cells maintain the desired lipid compositions in their two membrane leaflets.

In addition to the flippases, floppases, and scramblases, a wide variety of proteins with nonrelated primary functions can catalyze lipid flip-flop through different proposed mechanisms that include pore-mediated scrambling (14,15) and the so-called "credit-card" lipid movement (11). For some proteins, this secondary function has been proposed to have biological implications (16); for others, the physiological role (if any) remains unclear. Still, the ability of a variety of membrane proteins to scramble lipids has direct implications for the design and interpretation of studies using asymmetric protein-laden membranes and therefore should be carefully examined. A particularly interesting case is single-span transmembrane (TM) proteins that are often used to study protein-membrane interactions in vitro (17). Such proteins can facilitate lipid flip-flop through the so-called perturbation-mediated mechanisms, that is, lowering the energy barrier for lipid translocation between the leaflets by changing the bilayer structure and/or dynamics in the vicinity of the protein (18–22).

One single-span TM protein that reportedly affects lipid flip-flop only under certain conditions is the functional dimer configuration of the bacterial ion-channel gramicidin (gA) (23). To our knowledge, the channel has been shown to accelerate lipid translocation in three separate studies but to different extents: up to 30-fold in erythrocytes at moderate gA concentrations (gA/lipid ratio of ~1:200) (24); from 2- to 10-fold in supported lipid bilayers at high gA/lipid ratios (1:50) (25); and, to a somewhat lesser extent, in 400-nm-diameter liposomes with high gA ratios (1:20) in which flip-flop was unmeasurably slow in the absence of gA (14). At the same time, flip-flop enhancement was not detected in erythrocytes at gA concentrations at which the channel performs its ion-conducting function (24). The disparate results from these studies highlight limitations in the quantification of the transbilayer lipid distribution with rather indirect experimental methodologies, including extracting the outer leaflet lipids with albumin (which in its own right could perturb the bilayer) (24) or approximating the host lipid flip-flop kinetics from the translocation rate of a fluorescent lipid analog (14). The choice of system is also important: complex and asymmetric cell membrane environments like erythrocytes present challenges both for the interpretation of results and the quantification of the gA/lipid ratio, whereas the unavoidable bilayer defects in supported lipid bilayers prepared with the Langmuir-Blodgett/Langmuir-Schaefer technique could accelerate lipid flip-flop in a manner that is difficult to control (26).

Here, we address these challenges using a new (to our knowledge) platform for measuring protein-mediated lipid flip-flop in vitro. Our approach makes use of free-floating and stress-free large unilamellar vesicles with precisely controlled symmetric and asymmetric lipid composition, both in the presence and the absence of protein. This experimental setup allows for a wide range of biophysical assays and, importantly, enables the direct measurement of the flip-flop kinetics of unlabeled lipids in chemically symmetric and asymmetric bilayers using ^{1}H-NMR. This framework thus overcomes many of the limitations in the previous approaches by providing a robust model system for studying the effects of proteins on the transverse bilayer organization. Using this protocol, we examined the effect of gA on lipid flip-flop in both isotopically and compositionally asymmetric vesicles. Our results show that gA speeds up lipid translocation in both systems and that the rates are not directly proportional to gA concentration. Further computational analysis revealed that membrane deformations likely play a role in the observed effects at high gA mole fractions, suggesting the existence of mechanistically different regimes of gA-mediated changes in bilayer organization.

MATERIALS AND METHODS

Materials

All phospholipids (1-palmitoyl-2-oleoyl-*sn*-glycero-3-phosphocholine (POPC), 1-palmitoyl-2-oleoyl-*sn*-glycero-3-phospho-(1'-rac-glycerol) (POPG), POPC-d31, POPC-d13, 1,2-dimyristoyl-*sn*-glycero-3-phosphocholine (DMPC), and DMPC-d54; see Table 1 for a list of abbreviations) and gramicidin were purchased from Avanti Polar Lipids (Alabaster, AL) and Sigma-Aldrich (St. Louis, MO) respectively, as dry powders and used as supplied. The phospholipids were dissolved in high-performance liquid chromatography-grade chloroform, and gA was dissolved in high-performance liquid chromatography-grade methanol. Both phospholipids and gA were stored at −80°C until use. Methyl-β-cyclodextrin (MβCD), praseodymium(III) nitrate hexahydrate ($Pr(NO_3)_3$ $6H_2O$), sucrose, NaCl, and hydrochloric acid were purchased from Thermo Fisher Scientific (Waltham, MA). Thallium nitrate ($TlNO_3$) and 8-aminonaphthalene-1,3,6-trisulfonic acid disodium salt (ANTS) were purchased from Sigma-Aldrich (St. Louis, MO) and Invitrogen (Carlsbad, CA), respectively. Ultrapure H_2O

TABLE 1 List of Abbreviations

POPC	1-palmitoyl-2-oleoyl-*sn*-glycero-3-phosphocholine
POPC-d13	1-palmitoyl-2-oleoyl-*sn*-glycero-3-phosphocholine-1,1,2,2-d4-N,N,N-trimethyl-d9 (headgroup-deuterated POPC)
POPC-d31	1-palmitoyl-d31-2-oleoyl-*sn*-glycero-3-phosphocholine (chain-deuterated POPC)
DMPC-d54	1,2-dimyristoyl-d54-*sn*-glycero-3-phosphocholine (chain-deuterated DMPC)
POPG	1-palmitoyl-2-oleoyl-*sn*-glycero-3-phospho-(1'-rac-glycerol)
LUV	Large unilamellar vesicle
sLUV	Compositionally symmetric LUV
s*LUV	Compositionally symmetric but isotopically asymmetric LUV
aLUV	Asymmetric LUV
gA	Gramicidin A
gA-LUV	Large unilamellar vesicle with gA
gA-sLUV	Compositionally symmetric LUV with gA
gA-s*LUV	Compositionally symmetric but isotopically asymmetric LUV with gA
gA-aLUV	Asymmetric LUV with gramicidin
MLV	Multilamellar vesicle
MβCD	Methyl-beta-cyclodextrin
GC/MS	Gas chromatography/mass spectrometry
SAXS	Small-angle X-ray scattering
CD	Circular dichroism
GBFA	Gramicidin-based fluorescence assay
DSC	Differential scanning calorimetry
^{1}H-NMR	Proton nuclear magnetic resonance
MD	Molecular dynamics
CTMD	Continuum theory of membrane deformations
C_{out}	Area of shifted peak in ^{1}H NMR spectra after addition of shift reagent
C_{in}	Area of unshifted peak in ^{1}H NMR spectra after addition of shift reagent
ΔC	Difference between C_{out} and C_{in} relative to time 0, $(C_{out} - C_{in})/(C_{out}(0) - C_{in}(0))$
k_f	Rate of lipid flip-flop
$t_{1/2}$	Half time of lipid flip-flop

was obtained from a High-Q purification system (High-Q, Wilmette, IL), and D_2O (99.9%) was purchased from Cambridge Isotope Laboratories (Tewksbury, MA).

Preparation of liposomes without gA

Large unilamellar vesicles (LUVs) with symmetric lipid distribution (symmetric LUVs (sLUVs)) were prepared by first mixing appropriate volumes of lipid stocks in organic solvent with a glass Hamilton syringe. The solvent was evaporated with an Argon stream followed by high vacuum overnight. The dry lipid film was hydrated at room temperature (for POPC) or 35–40°C (for mixtures with DMPC) for at least 1 h with intermittent vortexing every 15 min. The resulting multilamellar vesicle (MLV) suspension was subjected to at least five freeze/thaw cycles using a −80°C freezer and then extruded through a 100-nm pore diameter polycarbonate filter with a mini-extruder (Avanti Polar Lipids) by passing the suspension through the filter 31 times. POPG was included in all sLUVs at 5 mol% to ensure unilamellarity (27).

Asymmetric LUVs (aLUVs) were prepared following the protocol described in (28) with slight modifications. Briefly, an MLV suspension of the donor lipid (i.e., the lipid to be exchanged into the outer leaflet of the aLUVs) was prepared in a 20% w/w sucrose solution as described above. The sample was diluted 20-fold with water and centrifuged at 20°C for 30 min at 20,000 × *g*. The supernatant was discarded, the pellet was redissolved using a 35 mM MβCD solution in water at a nominal donor lipid/MβCD ratio of 1:8, and the MβCD/donor mixture was incubated at room temperature for 2 h with gentle stirring. sLUVs of the acceptor lipids (i.e., the lipids to be present on the inner leaflet of the aLUVs) were prepared in a 25 mM NaCl solution as described above. These were added to the MβCD/donor mixture at a nominal donor/acceptor ratio of 2:1 or 3:1 (see Table S1). The MβCD/donor/acceptor slurry was incubated for 30 min at room temperature with gentle stirring. Immediately after this incubation, the sample was filtered with a prewashed centrifugal filter device (Ultra-15, 100,000 Da molecular weight cutoff; Amicon; MilliporeSigma, Burlington, MA) for 25 min at 2.5 K × *g*. The retentate was diluted with water eightfold and centrifuged for 30 min at 20,000 × *g* and 20°C to pellet the donor MLVs. The supernatant, containing aLUVs and residual MβCD, was carefully transferred to prewashed centrifugal filtration devices (as described above), concentrated to 250–500 μL, and washed with H_2O or D_2O a minimum of three times to remove MβCD. The aLUVs were recovered from the final retentate and stored in a plastic centrifuge tube at room temperature until further use.

Preparation of liposomes with gA

sLUVs with gA (gA-sLUVs) were prepared as follows. The lipids were first mixed in organic solvent, and gA was added from a methanolic solution with a glass Hamilton syringe at the appropriate gA/lipid ratio. The organic solvent was evaporated on a rotary evaporator, followed by high vacuum overnight. The dry sample was gently hydrated on a rotary evaporator for 30–60 min and then incubated at room temperature until the film was fully dissolved and the solution looked uniform (typically overnight). Vortexing was performed only occasionally and at the lowest setting. The sample was subjected to at least five freeze/thaw cycles using a −80°C freezer and then extruded with a 100-nm pore diameter polycarbonate filter as described above. POPG was added to all gA-sLUVs at 5 mol% to ensure unilamellarity.

aLUVs with gA (gA-aLUVs) were prepared following the protocol described above with the only modification that gA was added to the symmetric acceptor liposomes. That is, instead of acceptor sLUVs, acceptor gA-sLUV vesicles were added to the MβCD/donor mixture after the 2-h incubation. All other steps of the protocol were the same (see Fig. S1). The vesicle size distributions measured with dynamic light scattering showed little difference in LUV radius or polydispersity index between the symmetric acceptor vesicles and the final asymmetric vesicles (Table S2).

Gas chromatography-mass spectrometry

The overall lipid composition of the aLUVs and gA-aLUVs was determined from gas chromatography-mass spectrometry (GC/MS) analysis of fatty acid methyl esters (FAMEs) generated by acid-catalyzed methanolysis. The detailed protocol is described in (28). Briefly, ~100 μg of the sample was dried on a rotary evaporator, dissolved in 1 mL of 1 M methanolic HCl, flushed with Argon, and incubated at 85°C for 1 h in a glass culture tube sealed with a Teflon-lined cap. After allowing the sample to cool for a few minutes, 1 mL water was added, and the sample was briefly vortexed. Then, 1 mL hexane was added, and the sample was vortexed vigorously to form an emulsion and extract the FAMEs. The solution was centrifuged at a low speed (~400 × *g*) for 5 min to break the emulsion, and the upper (hexane) phase containing the FAMEs was transferred to a GC autosampler vial. The total volume in the vial was brought up to 1 mL with hexane. FAME analysis was performed using an Agilent 5890A gas chromatograph (Santa Clara, CA) with a 5975C mass-sensitive detector operating in electron-impact mode and an HP-5MS capillary column (30 m × 0.25 mm, 0.25-μm film thickness). After an injection of a 5-μL aliquot into the chromatograph, a preprogrammed column temperature routine was initiated as described in (28). Total ion chromatogram peaks were assigned and integrated using GC/MSD ChemStation Enhanced Data Analysis software. The ratio of the different lipid components was determined from the ratio of the respective peak areas of the FAMEs corresponding to the lipid fatty acid chains.

Small angle x-ray scattering

LUV samples for small angle x-ray scattering (SAXS) measurements were prepared as described above and concentrated to 15–20 mg/mL with prewashed centrifugal filter devices. SAXS measurements were performed using a Rigaku BioSAXS-2000 home source system with a Pilatus 100 K two-dimensional detector and a HF007 copper rotating anode (Rigaku Americas, The Woodlands, TX). SAXS data were collected at a fixed sample-to-detector distance using a silver behenate calibration standard, with a typical data collection time of 3–4 h. The one-dimensional scattering intensity $I(q)$ ($q = 4\pi\sin(\theta)/\lambda$, where λ is the x-ray wavelength and 2θ is the scattering angle relative to the incident beam) was obtained by radial averaging of the corrected two-dimensional image data, an operation that was performed automatically using Rigaku SAXSLab software. Data were collected in 10-min frames with each frame processed separately to assess radiation damage; there were no significant changes in the scattering curves over time. Background scattering from water collected at the same temperature was subtracted from each frame, and the background-corrected $I(q)$ from the individual frames was then averaged with the SD taken to be the measurement uncertainty. Scattering data analysis is described in detail in the Supporting Materials and Methods.

Circular dichroism

Samples for circular dichroism (CD) were first diluted to 1 mg/mL lipid concentration for a protein concentration between 5 and 13 μM. The lipid concentration was estimated from dynamic light scattering (DLS). gA conformation was measured using a J-815 spectropolarimeter equipped with a PTC-423S Peltier temperature controller (Jasco, Easton, MD). CD spectra (raw ellipticity θ in units of millidegree versus wavelength) were collected at 25°C using a 2-mm path-length cuvette, a scan rate of 100 nm/min, and 30 accumulations. The spectrum of each gA-containing sample was first corrected for the lipid background by subtracting the spectrum of a corresponding lipid-only sample. The only exception was the gA-aLUV sample, for which the background was taken to be the spectrum of the POPC acceptor sLUVs, which were similar in size to the gA-aLUVs as determined from DLS. The background-corrected data were then converted to mean residue molar ellipticity $[\theta]$ (in units of degree cm^2 dmol^{-1}) using the relationship

$$[\theta] = \frac{10^6\theta}{lcN_{aa}}, \tag{1}$$

where l is the cell path length in mm, c is the protein concentration in μM, and $N_{aa} = 15$ is the number of amino acids in the gA protein.

gA-based fluorescence assay

gA function was quantified using a fluorescence quench protocol (29). For these studies, the acceptor sLUVs were prepared with a gA/lipid ratio of 1:20,000 (corresponding to 7–8 gA monomers per 130-nm diameter vesicle) and hydrated with 25 mM Na_2ANTS instead of 25 mM NaCl. After the last concentration step, the gA-aLUVs were washed once with H_2O and three times with elution buffer (35 mM $NaNO_3$ and 6 mM HEPES (pH 7.0)). The rate of quenching of the ANTS trapped inside the vesicles was measured using a stopped-flow spectrofluorometer (SX.20; Applied Photophysics, Leatherhead, UK) in a single-mixing experiment and quantified with a regular stretched exponential (29). The ANTS-loaded LUVs were mixed with either $NaNO_3$ buffer (35 mM $NaNO_3$ and 6 mM HEPES (pH 7.0)) or $TlNO_3$ buffer (35 mM $TlNO_3$ and 6 mM HEPES (pH 7.0)), in which Tl^+ (thallous ion) is a gA channel-permeant quencher of the ANTS fluorescence. The samples were excited at 352 nm, and the fluorescence signal above 455 nm was recorded in the absence (four successive trials) or the presence (nine successive trials) of the quencher. As a control, gA-sLUV acceptors hydrated with ANTS were also washed three times with elution buffer, and the rate of ANTS quenching was measured as described above.

Differential scanning calorimetry

Samples for differential scanning calorimetry (DSC) were diluted to ~5 mg/mL and measured using a Nano DSC (TA Instruments, New Castle, DE). The LUV suspension was loaded into the sample capillary cell, and degassed solvent was loaded into the reference capillary cell. The cells were pressurized to 3 atmospheres to suppress the formation of air bubbles, and a cooling scan was initiated from 30°C to −8°C at a rate of 0.2°C/min. All thermograms showed either a series of peaks or a single broad peak between ~−5 and 20°C. A sloping background contribution was accounted for by fitting a portion of the thermogram on either side of the peaks of interest to a third-order polynomial, which was then subtracted from the raw data.

^{1}H-NMR

The interleaflet lipid distribution in the aLUVs and gA-aLUVs was quantified with a shift reagent assay performed on either a Bruker Avance III 400 MHz spectrometer (Bruker, Billerica, MA) (at Oak Ridge National Laboratory, Oak Ridge, TN) or a Bruker Avance III HD 500 MHz spectrometer (at Weill Cornell Medical College, New York, NY) as described in (26,28). Briefly, a standard ^{1}H pulse sequence with a 30° flip angle and a 2-s delay time was collected at 35°C. For all samples measured in H_2O, the signal from the solvent was suppressed using the standard excitation sculpting sequence *zgesgp*. A sample aliquot was first diluted with D_2O or H_2O to a total volume of 600 μL and a concentration of ~0.5 mg/mL. The diluted sample was loaded into an NMR tube, and a spectrum was recorded. A small aliquot (1–2 μL) of 20 mM Pr^{3+}/D_2O was then added to the NMR tube and mixed with its contents by inverting the tube three times ($[Pr^{3+}] \approx 50$ μM), and the spectrum was recorded immediately thereafter; another aliquot of Pr^{3+} was added, and the procedure was repeated. A total of at least three Pr^{3+} titrations were performed, and their spectra were recorded and used to establish the measurement uncertainty as described below. The typical elapsed time between the first exposure of the sample to Pr^{3+} and completion of the experiment was 40 min. Each Pr^{3+} titration resulted in a further shift of the resonance peak of the protiated choline headgroups exposed on the outer leaflet of the vesicles as shown in Fig. S2.

NMR analysis was performed by fitting each spectrum as a sum of Lorentzians using Origin or custom Mathematica scripts. The choline resonances were identified, and the fraction of exposed (i.e., outer leaflet) and protected (i.e., inner leaflet) choline headgroups was quantified from the areas of the shifted and unshifted choline peaks and used to determine the fraction of protiated-headgroup lipid in each leaflet. The measurement uncertainty was calculated as the SD of peak areas determined from the Pr^{3+} titration data described above. This information, together with the GC results, was used to calculate the composition of the two bilayer leaflets as described previously (28,30).

Analysis of lipid flip-flop kinetics

The rate of lipid flip-flop, k_f, was measured from the time-dependent changes in the transverse distribution of protiated-headgroup lipids in each sample as described in (26). Briefly, the NMR time traces of relative changes in the lipid distribution were expressed as

$$\Delta C(t) = \frac{C_{out}(t) - C_{in}(t)}{C_{out}(0) - C_{in}(0)}, \tag{2}$$

where $C(t)$ is the area of the shifted (outer leaflet) and unshifted (inner leaflet) choline peaks at time t, with subscripts *out* and *in* denoting the outer and inner leaflet, respectively. The data were modeled as

$$\Delta C(t) = e^{-2k_f t}, \quad (3)$$

with the corresponding half-time $t_{1/2}$ given by

$$t_{1/2} = \frac{\ln(2)}{2k_f}. \quad (4)$$

All samples were kept on the bench between NMR measurements, and consequently, the flip-flop kinetics reported here correspond to sample behavior at an ambient temperature of ~22°C.

Molecular dynamics simulations

All-atom molecular dynamics (MD) simulations of gA in the symmetric and compositionally asymmetric bilayers from the in vitro experiments were performed as described below.

For the symmetric system, a POPC bilayer with 100 lipids per leaflet (200 lipids total) was first constructed with CHARMM-GUI (31–33). The bilayer was hydrated with 70 waters per lipid and a total of 35 Na^+ and 35 Cl^- ions for a salt concentration of 138 mM. After a short initial equilibration with CHARMM-GUI's protocol, the system was run for 226 ns. From the last frame of the trajectory, all water and ion atoms were removed, and a single gA dimer (Protein Data Bank [PDB]: 1JNO) was manually inserted in the bilayer by replacing ten lipids from each leaflet with a gA monomer. The system was then hydrated and ionized with VMD's solvate and autoionize plugins, respectively, resulting in a bilayer patch with 90 lipids per leaflet (180 lipids total), 1 gA dimer, 67 waters per lipid, and 30 Na^+ and 30 Cl^- ions for a salt concentration of 138 mM NaCl.

For the asymmetric system, the protocol in (34) was used to identify the appropriate number of lipids in the asymmetric lipid-only bilayer with the top leaflet composed of DMPC/POPC 75/25 mol% and the bottom leaflet composed of DMPC/POPC 10/90 mol%. The resulting tension-free bilayer contained 104 and 100 lipids in the top and bottom leaflets, respectively, and was constructed and equilibrated with CHARMM-GUI's protocols. After a production run of 445 ns, gA was manually inserted in the bilayer by removing eight lipids from each leaflet while maintaining the overall leaflet compositions. The system was hydrated with VMD's solvate plugin, resulting in a bilayer patch with 96 lipids in the top leaflet, 92 lipids in the bottom leaflet, 1 gA dimer, and 55 waters per lipid.

All simulations were performed with the NAMD software (35) and the CHARMM36 force field for lipids (36,37) in the NPT ensemble under constant pressure of 1 atmosphere and a temperature of 25°C. The force-field parameters for gA were kindly provided by Andrew Beaven and were based on those used in (38), made compatible with the CHARMM36 force field. Namely, the D-amino acids were treated in the same way as L-amino acids (except for their chirality), whereas the parameters for the gA terminal residues (formyl and ethanolamine) were the same as in (38) with the particular atom types renamed to conform to the CHARMM36 atom notation. For both the symmetric and asymmetric bilayers with gA, the system was first energy minimized for 10^4 steps and then run for 100 ps with a 1-fs time step. After this initial relaxation, the POPC/gA bilayer was simulated for 887 ns, and the asymmetric bilayer with gA was simulated for 705 ns with a 2-fs time step. Additional details of all simulated systems and the corresponding simulation parameters are found in Supporting Materials and Methods, Section S1.

Quantification of membrane deformation from simulations

To quantify the deformation of the membrane around gA, the trajectories were first centered and aligned on the backbone of gA. Because gA can tilt with respect to the bilayer normal in the course of the simulations, special care was taken to ensure that the alignment step did not result in abnormal tilting of the membrane, effectively leading to artificial changes in the bilayer thickness in the vicinity of the protein. The gA-lipid boundary was identified separately for each leaflet as the outermost layer of the time-averaged occupancy map (constructed on a 2 × 2 Å grid) of the respective gA monomer atoms projected onto the x-y plane. The leaflet thickness at the gA-lipid boundary was calculated from the interpolated z positions of the lipid atoms in the respective grid points as described in Supporting Materials and Methods, Section S2. The leaflet thickness at the gA-lipid boundary was used to obtain the optimal deformation profile around a gA monomer by a self-consistent free-energy minimization procedure as described in Supporting Materials and Methods, Section S3. The leaflet deformation around gA at distance r from the gA center was calculated as the squared deviation in the thickness averaged over the area between the grid points at distance r from the gA center and the gA-lipid boundary (the bulk leaflet thickness was taken from the corresponding lipid-only simulations). The membrane deformation was taken as the sum of the deformations of the two leaflets.

Quantification of membrane deformation in experiments

To estimate the amount of membrane deformation at each of the gA/lipid ratios used in the experiments, we first approximated the number N_{gA} of gA dimers on a vesicle from the following: 1) the total surface area of a vesicle with diameter 130 nm (the average vesicle size measured with DLS), 2) the average area per lipid 64 $Å^2$ (calculated from MD simulations for a POPC bilayer), and 3) the area per gA monomer 208 $Å^2$ approximated from the occupancy map of the gA monomers described above. N_{gA} gA dimers were then distributed uniformly on the surface of a sphere with diameter 130 nm using MATLAB (The MathWorks, Natick, MA), and the distance d between them was recorded. The membrane deformation at a given gA/lipid ratio was estimated as the membrane deformation at a distance $d/2$ from the gA center.

RESULTS

gA incorporation is similar in symmetric and asymmetric liposomes

We modified a recently developed protocol for the construction of asymmetric lipid-only vesicles (28,30) to enable the preparation of asymmetric proteoliposomes. As described in Materials and Methods, the protocol involves mixing two populations of symmetric vesicles (only one of which contains preincorporated protein) and exchanging the lipids between their outer leaflets with MβCD (Fig. S1). Using this procedure, we prepared two types of gA-containing vesicles: 1) compositionally symmetric but isotopically asymmetric liposomes (s*LUVs) with an inner leaflet composed of POPC or its headgroup-perdeuterated variant (POPC-d13) and an outer leaflet exchanged with its chain-perdeuterated variant (POPC-d31); and 2) compositionally asymmetric vesicles (aLUV) with the same inner leaflet composition as above and an outer leaflet exchanged with the chain-perdeuterated variant of DMPC (DMPC-d54). Table S1 shows the donor mole fraction in the final samples as determined from GC/MS (see Materials and Methods), which ranged between 0.32 and 0.4 for the s*LUVs and between 0.35 and 0.45 for the aLUVs. The size of the vesicles

was measured with DLS and was on average 130 nm in diameter with polydispersity index of <0.2 (Table S2).

We used SAXS to examine the effect of gA incorporation on bilayer structure. Fig. 1 *A* shows scattering intensity versus momentum transfer vector q for POPC LUVs with an increasing concentration of gA from 0 to 2.5 mol%. The curves exhibit the typical lobes of coherent scattering separated by distinct minima that is characteristic of the core-shell structure of lipid bilayer vesicles (39). The most notable feature is a nearly linear increase in the scattering intensity near the minimum at $q \sim 0.28$ Å^{-1} with increasing gA concentration. To better understand the origin of this liftoff, we used Monte Carlo simulations to calculate SAXS curves corresponding to vesicles with randomly dispersed gA TM dimers (see Supporting Materials and Methods, Section S4 for additional details of simulation methods and results). Simulated SAXS curves for vesicles with increasing gA concentration, shown in Fig. 1 *B*, precisely reproduced the enhanced scattering, conclusively demonstrating that this feature arises from an electron density contrast between the lipid bilayer and a TM protein. We also simulated the effect of gA aggregation within the bilayer. Fig. S11 reveals that lateral association of gA channels rapidly diminishes the liftoff, with the largest effect occurring upon lateral dimerization. Aggregates of three or more gA channels largely abrogate the liftoff, resulting in SAXS curves that are practically indistinguishable from a gA-free vesicle. A comparison of the experimental SAXS data from the gA-s*LUVs to curves from the symmetric gA concentration series (Fig. 1 *A*) suggests that little if any gA was lost from acceptor vesicles during CD-mediated lipid exchange and that gA is not laterally aggregated within the vesicles.

Although our initial goal was to use SAXS to look for changes in bilayer structure induced by gA, we did not observe any significant shift in the positions of the scattering minima that typically accompany changes in bilayer thickness. We conducted additional Monte Carlo simulations to determine the sensitivity of SAXS to perturbations in the first shell of ~14 lipids surrounding each gA channel. Fig. S12 shows only minor differences in SAXS curves upon changing the area per lipid of the first shell by 10 Å^2 at a gA concentration of 2.5 mol%. Indeed, no significant change at all is seen for a perturbation from 64 to 70 Å^2, which would correspond to a ~3.5 Å thinning of the surrounding bilayer induced by gA. These simulations suggest that, at least for the experimental conditions used here, it is not possible to draw conclusions from SAXS data about small local bilayer perturbations induced by gA.

gA conformation and function are the same in symmetric and asymmetric liposomes

Next, we examined the structural properties of the incorporated gA. In addition to its canonical helical dimer conformation, gA can exist in other nonfunctional conformations, such as a dimeric helix in which two gA monomers are intertwined into a single extended helix (40). The dimeric helix conformation can arise from a hydrophobic mismatch (or from storing gA in some nonpolar solvents) and has a distinct CD spectrum (41). Fig. S3 shows the CD spectrum of gA in the aLUVs in comparison with the spectra of gA in sLUVs made of either just POPC or DMPCd54. The data show that most of the 2.5 mol% gA in the symmetric samples was in a helical dimer conformation and that this conformation remained unchanged during the steps of the gA-aLUV preparation protocol.

To evaluate the function of gA in the asymmetric liposomes, we measured the rate at which a fluorophore (ANTS) trapped inside the vesicles was quenched by an externally added quencher (thallium, Tl^+). This assay provides a measure of the equilibrium dimer-to-monomer ratio of gA in the bilayer by taking advantage of the fact that Tl^+

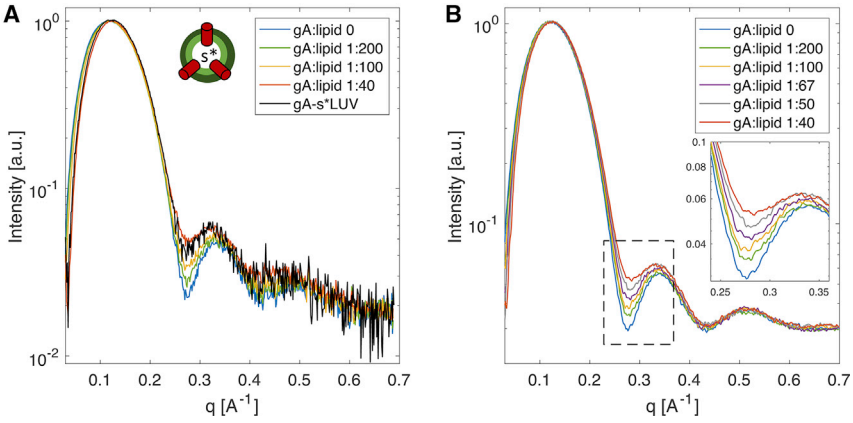

FIGURE 1 Gramicidin incorporation is similar in symmetric and asymmetric liposomes. (*A*) Experimental SAXS form factors of a series of POPC gA-sLUVs with an increasing concentration of gA and isotopically asymmetric LUVs, gA-s*LUV, composed of deuterated variants of POPC and prepared with a nominal gA/lipid ratio of 1:40. The cartoon schematic next to the figure legend represents an isotopically asymmetric gA-s*LUV. All measurements were performed at 25°C. (*B*) SAXS form factors calculated from Monte Carlo simulations of a POPC vesicle with different concentrations of gA (see Supporting Materials and Methods). The increase in the intensity at the minimum between the first and second scattering lobes with increasing gA concentration (shown in an expanded view in the *inset*) is caused by the electron density contrast between the lipid bilayer and the membrane-spanning gA dimers. To see this figure in color, go online.

can enter the vesicles and quench ANTS only through functional gA dimers (29). Fig. 2 *A* shows the ANTS fluorescence decay as a function of time in the initially symmetric acceptor vesicles (66.1 s^{-1}) and the final isotopically asymmetric gA-s*LUVs (62.9 s^{-1}). The ratio of the two rates (0.95) indicates that the dimer/monomer equilibrium of gA in the isotopically asymmetric vesicles was essentially unaffected by the cyclodextrin-mediated lipid exchange. We obtained a similar ratio of 0.99 for the compositionally asymmetric liposomes (Fig. 2 *B*), confirming that in both asymmetric samples, gA function remained intact.

gA scrambles lipids in compositionally asymmetric vesicles

That gA can scramble lipids first became evident in DSC experiments, in which thermodynamic phase transitions (such as transitions between gel and fluid) are detected by monitoring the release of heat from a sample as a function of temperature. Fig. 3 shows a cooling temperature scan performed after sample preparation (scan 1) for compositionally asymmetric vesicles without (Fig. 3 *A*) and with (Fig. 3 *B*) gA (see Materials and Methods). Two transition peaks are visible in both samples, likely coming from the different melting temperatures of the POPC-rich inner leaflet and the DMPC-d54-rich outer leaflet (the main transition temperatures of POPC and DMPC-d54 are −2 and 19°C, respectively; see Fig. S4). After the first scan, the temperature was again brought to 30°C, and a second cooling scan (scan 2) was performed without any observable changes in the DSC spectra, indicating that cycling through the temperature range of −8 to 30°C (and consequently, through the gel-liquid crystalline transition of each leaflet) by itself did not result in any major redistribution of the lipids between the two leaflets. In the gA-aLUV sample, however, after a set of fixed temperature incubations (20°C for 12 h, followed by 45°C for 5 h), the two peaks began to merge (scan 3, Fig. 3 *B*), whereas those of the aLUV sample without gA remained unchanged (scan 3, Fig. 3 *A*). The changes in the gA-aLUV sample were even more pronounced after subjecting the samples to another set of fixed temperature incubations (scan 4). These results indicate that gA facilitated the exchange of lipids between the two leaflets, presumably through its ability to accelerate lipid flip-flop, which eventually would result in a symmetric bilayer with a single transition temperature peak (*gray dashed lines* in Fig. 3).

gA increases the rate of lipid flip-flop in compositionally asymmetric vesicles

To quantify the effect of gA on lipid flip-flop, we used ^{1}H-NMR to measure the rate of lipid translocation in the presence and the absence of the channel (see Materials and Methods). The nine equivalent protons on a protiated choline headgroup produce a clearly defined resonance peak at 3.1–3.6 ppm. The shift reagent Pr^{3+}, when added externally to the sample, interacts only with the lipid headgroups exposed on the outer leaflet of the vesicles and shifts their resonance downfield (26,42). (We further confirmed that Pr^{3+} does not alter bilayer properties using the fluorescence quenching assay mentioned above; see Table S3.) After exchanging lipids with protiated choline headgroups (POPC-d31 or DMPC-d54) into acceptor vesicles composed of the headgroup-deuterated POPC-d13, the only detectable resonance comes from the exchanged donor lipids that are initially in the outer leaflet. The distribution of the protiated-headgroup lipids across the two bilayer leaflets thus can be determined from the ratio of the areas of the shifted and unshifted choline peaks in the NMR spectrum. Repeating the shift experiment on different aliquots of the sample over time allows for direct quantification of the lipid flip-flop rate (26). To minimize the exposure of the LUVs to Pr^{3+}, the sample was incubated at room temperature in the absence of Pr^{3+}; the shift reagent was added to a sample aliquot immediately before the NMR measurement, and

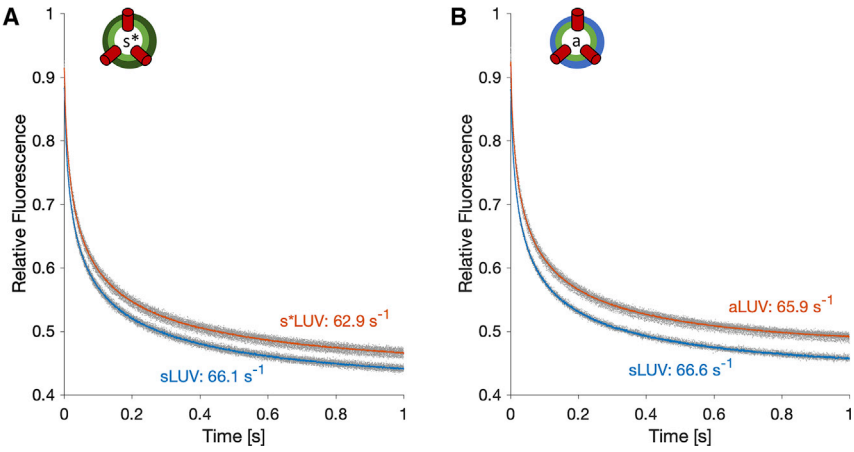

FIGURE 2 Gramicidin channel function remains intact in asymmetric liposomes. Changes in ANTS fluorescence over time for the isotopically (*A*) and compositionally (*B*) asymmetric samples (in *red*) and their corresponding symmetric acceptor vesicles (in *blue*). Replicate traces are shown in gray; their averages are shown in color. The fluorescence signal was normalized to the fluorescence measured before the addition of Tl^+. The average rates calculated from the traces are indicated next to each trace. The cartoon schematic in (*B*) represents a compositionally asymmetric gA-aLUV. All measurements were performed at an ambient temperature of ~22°C. To see this figure in color, go online.

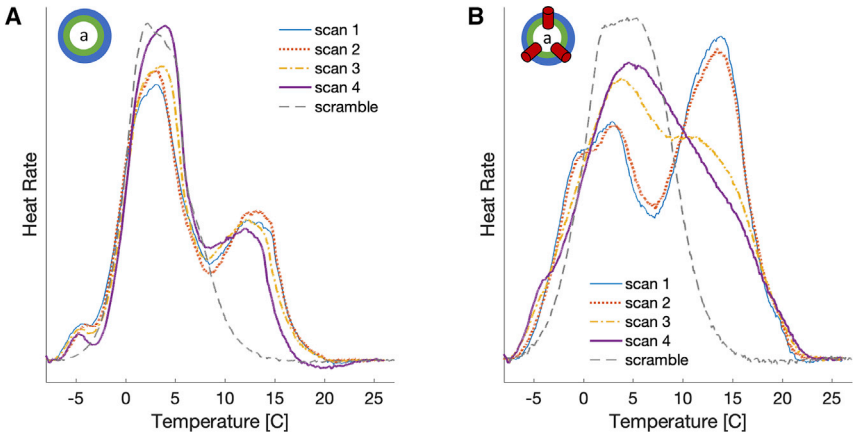

FIGURE 3 Gramicidin scrambles lipids in compositionally asymmetric vesicles. DSC data of compositionally asymmetric LUVs with DMPC-d54 and POPC and without (*A*) or with (*B*) gramicidin at gA/lipid ratio of 1:40 are shown. Four consecutive cooling scans were performed as follows: after the asymmetric vesicle preparation (scan 1, *thin blue line*), after scan 1 (scan 2, *dotted red line*), after subsequent incubation at 20°C for 12 h followed by incubation at 45°C for 5 h (scan 3, *dash-dotted yellow line*), and after another set of incubations at 20°C for 12 h and 45°C for 5 h (scan 4, *thick purple line*). Also shown for comparison with gray dashed lines are data for the symmetric samples (scramble) with the same overall composition as the asymmetric vesicles (Table S1). To see this figure in color, go online.

the aliquot containing Pr^{3+} was discarded after measurement as described in Materials and Methods. The main transition temperature T_M of DMPC-d54 (the DMPC variant used in these experiments) is less than 20°C (see Fig. S5) in contrast to fully protiated DMPC (T_M = 24°C). As a result, the asymmetric samples both with and without gA were fully in the fluid phase at room temperature (Fig. 3).

Fig. 4 shows the relative changes in transverse lipid distribution ΔC (see Eq. 2) as a function of time for both the chemically symmetric (Fig. 4 *A*) and asymmetric (Fig. 4 *B*) liposomes with different amounts of gA (see Materials and Methods). Table 2 lists the corresponding lipid flip-flop rates and half times calculated as described in Materials and Methods. Whereas the spontaneous lipid flip-flop rate in the absence of gA is immeasurably slow in the s*LUVs, it is markedly increased when DMPC is exchanged into the outer leaflet of POPC (Fig. 4, *A* and *B*, *black squares* and *curves*). Importantly, the rate of lipid translocation in both samples increases in the presence of the channel in a manner that depends on gA concentration.

Models for gA-mediated lipid flip-flop

If each additional gA dimer accelerated the movement of a constant, fixed number of lipids between the leaflets, the rate of lipid flip-flop would vary linearly with gA mole fraction (20). Fig. 5 shows the flip-flop rates calculated from the NMR data (Table 2) as a function of the gA/lipid ratio. Indeed, the data for the s*LUV samples (shown in *blue*) are consistent with the model of single gA channel-mediated lipid translocation. However, in the aLUV samples (shown in *red*), the linear relationship predicted from the model is not as clear, and the uncertainty in the data precludes any firm conclusions. Considered together, the two data sets introduce a conundrum: in the absence of gA, the flip-flop rate in the compositionally asymmetric bilayers is clearly faster than the rate in the symmetric membranes, yet in the presence of gA at a gA/lipid ratio of 1:40, this trend is reversed and the flip-flop kinetics in the aLUVs are much slower than those in the s*LUVs. This result suggests a mechanism different from a single channel-induced perturbation, by which gA catalyzes lipid translocation, based

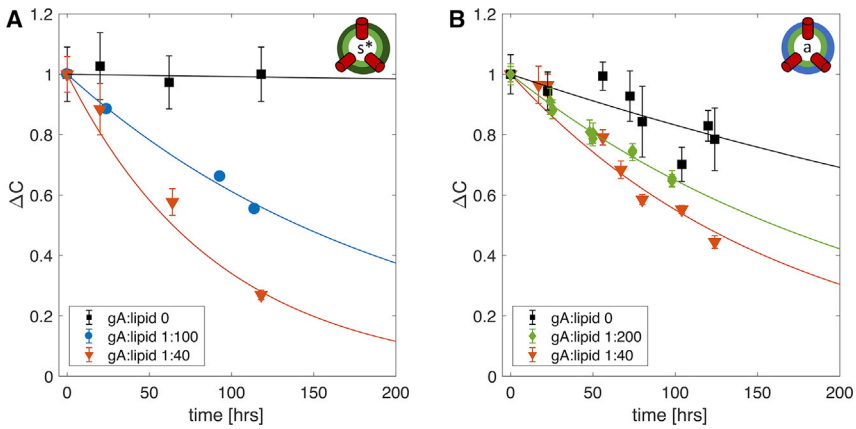

FIGURE 4 Gramicidin increases the rate of lipid flip-flop in isotopically and compositionally asymmetric vesicles. The time evolution of the interleaflet distribution of POPC-d31 in s*LUVs (*A*) and DMPC-d54 in aLUVs (*B*) either without gA (*black squares*) or with gA at a gA/lipid ratio of 1:40 (*red triangles*), 1:100 (*blue circles*), and 1:200 (*green diamonds*). Both plots show the time-dependent changes in the distribution of POPC-31 between the outer and inner leaflets, relative to the first time point measured after vesicle preparation (ΔC). See text for details. Error bars represent SDs of at least three consecutive Pr^{3+} additions. Each time trace in (*A*) is from a single sample. The time traces of the compositionally asymmetric vesicles in (*B*) are from one (gA/lipid 1:40), two (no gA), and three (gA/lipid 1:200) separately prepared samples, respectively. The kinetics reported here corresponds to sample behavior at an ambient temperature of ~22°C. To see this figure in color, go online.

TABLE 2 Translocation Kinetics in the Examined Systems

Outer Leaflet	gA/lipid	$t_{1/2}$ [h]	$k_f/10^{-7}$ s^{-1}
POPC-d31/	0	~8900	~0.1
POPC-d13	1:100	141 [125; 163]	6.8 [5.9; 7.7]
	1:40	64 (55; 76)	16.0 [12.6; 17.4]
DMPC-d54/	0	376 [251; 748]	2.6 [1.3; 3.8]
POPC-d13	1:200	160 [153; 168]	6.0 [5.7; 6.3]
	1:40	116 [104; 132]	8.3 [7.3; 9.2]

Shown are the corresponding half times and the rates of lipid flip-flop calculated from the NMR data shown in Fig. 4 as described in Materials and Methods. The numbers in brackets represent 95% confidence intervals.

on the following considerations: 1) because the gA channel is relatively short, it is likely to cause thickness deformations in the membrane; and 2) the thickness deformations in a POPC bilayer could be alleviated in the presence of a shorter-chain lipid like DMPC. Thus, gA-induced bilayer stress is likely a contributing factor to the observed trends.

Membrane deformations are likely to play a role in gA-mediated lipid flip-flop

gA has been routinely used as a model peptide to study local bilayer deformations that result from protein-membrane interactions (43,44). In this context, it is important that the gA channel's helical pitch is invariant with respect to changes in the channel-bilayer hydrophobic mismatch, meaning that the bilayer will adjust to the channel rather than the channel adjusting to the bilayer (in bilayers having a hydrophobic thickness greater than the channel length) (45). gA has been shown to induce thinning in a pure DMPC bilayer (46), and one would expect the same effect in bilayers with a hydrophobic thickness greater than DMPC, such as

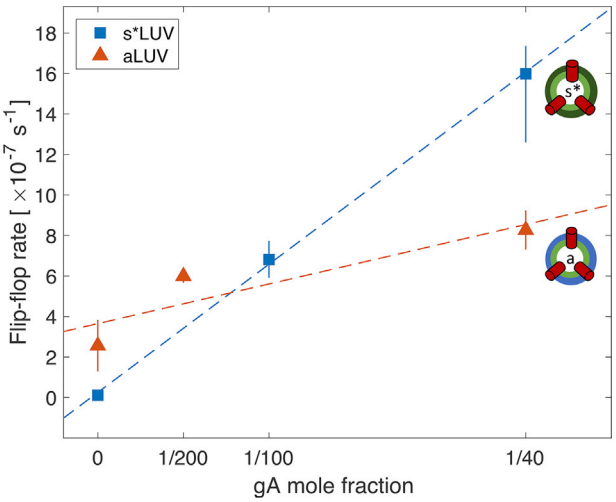

FIGURE 5 The rate of lipid flip-flop shows a complex relationship with gA mole fraction. Flip-flop rates were calculated from the data in Fig. 4 for the compositionally symmetric (*blue squares*) and asymmetric (*red triangles*) LUVs (see Table 2) as a function of the nominal gA mole fraction in the samples. Error bars represent 95% confidence intervals. To see this figure in color, go online.

a membrane composed of POPC (47). Such local deformations produce stress on the membrane that will increase with an increasing gA concentration and could potentially affect lipid flip-flop. We therefore investigated the response of the bilayer to the presence of a single gA channel in the two experimentally studied systems.

MD simulations, in combination with the continuum theory of membrane deformations (CTMD) (48), were used to estimate the amount of membrane deformation at the different gA mole fractions from the experiments. This was achieved by first quantifying the changes in membrane thickness as a function of distance from the channel and then relating them to the average distances between channels in the samples. To enable these calculations, MD simulations were performed on a system containing a single gA channel embedded in a symmetric POPC bilayer or in an asymmetric membrane with a top leaflet of DMPC/POPC 0.75/0.25 and a bottom leaflet of DMPC/POPC 0.10/0.90. The compositions of the two leaflets were based on a different set of samples prepared for small-angle neutron scattering experiments (unpublished data) and were similar to the leaflet compositions of the samples examined with NMR in this work (Table S1). At the end of the simulations, the thickness of each leaflet at the gA-lipid boundary was analyzed and used to calculate the optimal thickness deformation profile around gA using the CTMD formalism as described in Materials and Methods and Supporting Materials and Methods, Section S3. Because the membrane deformation energy varies with the square of the hydrophobic mismatch (Eq. S3), Fig. 6 *A* shows the resulting average squared deviations in thickness as a function of distance from the gA center in both systems. The amount of membrane deformation decreases gradually further away from the protein in the two bilayers, and it is less in the asymmetric membrane, indicating that gA is able to adapt more easily to the asymmetric bilayer environment.

To examine whether membrane deformations could be involved in the ability of gA to scramble lipids, we approximated the packing density of gA dimers within the experimentally prepared LUVs. We estimated the distance between the channels at each gA mole fraction by assuming that they are uniformly distributed on the surface of the vesicles (see Materials and Methods). The dotted lines on Fig. 6 *A* indicate the respective half distances between the gA centers. The compositionally symmetric sample with gA at a gA/lipid ratio of 1:40, in which the rate of lipid flip-flop was highest (Table 2), also seemed to have the largest membrane deformation (as determined from the MD simulations) among the examined asymmetric proteoliposomes. Fig. 6 *B* shows the relationship between the measured rates of lipid flip-flop in the four gA-aLUVs and the corresponding amounts of membrane deformation as quantified by the analysis in Fig. 6 *A*. Whereas the correlation between gA-mediated lipid scrambling and membrane deformation at gA mole fractions $\geq$0.01 is very strong

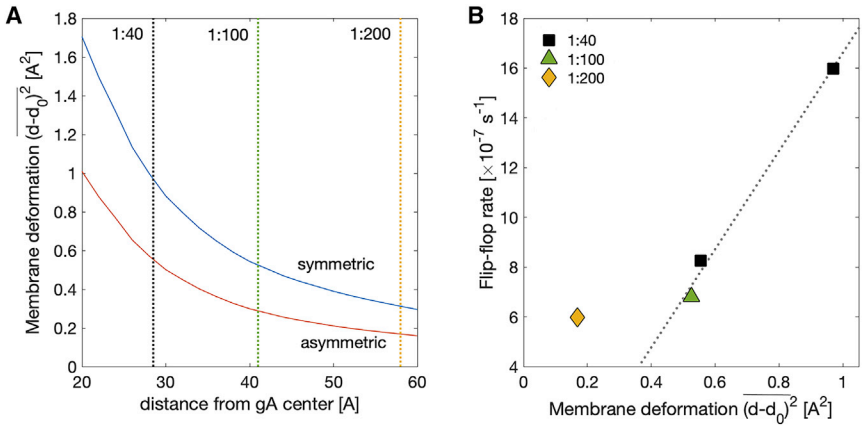

FIGURE 6 The gA-mediated lipid flip-flop rate at high gA concentrations correlates with membrane deformation. (*A*) Average squared deviations in bilayer thickness as a function of distance from gA center for a symmetric POPC bilayer and an asymmetric bilayer as in the NMR experiments in Fig. 4. The thickness deviations were calculated from the membrane deformation profiles around a single gA channel obtained by a CTMD-guided free-energy minimization utilizing information from MD simulations (see Materials and Methods). Dotted lines indicate the approximated half distances between gA channels on the surface of the LUVs at three different gA/lipid ratios: 1:40 (*black*), 1:100 (*green*), and 1:200 (*yellow*). (*B*) gA-mediated lipid flip-flop rate from Fig. 5 as a function of the corresponding membrane deformation from (*A*). The data points denote different gA/lipid mole ratios: 1:40 (*black square*), 1:100 (*green triangle*), and 1:200 (*yellow diamond*). To see this figure in color, go online.

(0.998), the sample with a gA/lipid ratio of 1:200 did not follow the same relationship and appeared as an outlier (Fig. 6 *B*). This result suggests that the stress induced in the membrane as a result of gA-membrane interactions is an important contributor to the observed effects of gA on lipid scrambling and that at high mole fractions, the channels accelerate lipid flip-flop in a mechanistically different way than at low gA concentrations. We note that the same qualitative results for the gA-induced flip-flop rate and membrane deformation are obtained, even assuming a 20% loss of gA during the preparation of asymmetric vesicles (an upper limit estimated from the SAXS data).

DISCUSSION

In studies of protein-membrane interactions, the effects of the membrane (e.g., its composition and structure) on protein function and oligomerization have been examined extensively. It is equally important, however, to account for the protein's effect on the membrane because a protein embedded in a bilayer is prone to introduce defects that can perturb the bilayer structure and affect its transverse and lateral organization. We have, therefore, developed, to our knowledge, new protocols for the systematic investigation of protein-mediated changes in the lipid compositions of the two bilayer leaflets by utilizing model systems that allow for fine tuning of various membrane parameters. As discussed below, these protocols have been devised to exploit biophysical properties that bring to light specific elements of the complex interplay between the protein and the membrane and to quantify the consequences.

In the following, we first discuss the preparation and properties of the gA-containing asymmetric lipid vesicles; we then turn to the effect of gA on lipid flip-flop; and, finally, we present a possible mechanism for the gA-induced lipid scrambling observed in the experiments.

Preparation and biophysical characterization of asymmetric proteoliposomes

Asymmetric membranes containing TM proteins have been successfully prepared in the past using two general approaches. In one, the protein (either soluble or micelle stabilized) is added externally to preformed asymmetric membranes, including LUVs filled with sucrose (49), droplet interface bilayers (50), and planar supported bilayers (51). In the other (also used here), the protein is first reconstituted into symmetric vesicles, after which the outer leaflet lipids are exchanged with different lipids. For example, using the latter approach, Vitrac et al. prepared sonicated small unilamellar vesicles (SUVs) with the 12 TM protein LacY from *Escherichia coli* and examined the effect of asymmetric charge distribution on the topology of the protein (4,52). In a different study, asymmetric SUVs containing the nicotinic acetylcholine receptor were prepared by using MβCD-loaded lipid complexes to exchange the lipids on the outer leaflet of symmetric SUVs containing nicotinic acetylcholine receptor with sphingomyelin (3). Although these examples illustrate how a variety of TM proteins can be incorporated into asymmetric model membranes of different geometries, the effect of the protein (and protein incorporation) on the lipid compositions of the two bilayer leaflets can vary and therefore has to be examined explicitly.

To this end, the protocols and assays presented here offer an advantageous platform for biophysical characterization of the sample, much improved by utilizing large tensionless proteoliposomes that are free from the potential effects of curvature, residual organic solvent, or polymer cushion supports. Indeed, we found only minimal effects of the preparation protocol on the incorporation, conformation, and function of gA (Figs. 1, 2, and S3). Still, these effects are likely to depend on the types of lipids in the vesicles, and their negligible magnitude cannot be taken for granted. For example, the energetic cost of gA dimer formation

increases with increasing bilayer thickness, resulting in a shift of the gA monomer/dimer equilibrium toward the monomeric state (41,53); in such cases, the gA monomers have been shown to more easily exchange between vesicles (54). This could result in a partial loss of the protein during the CD-mediated lipid exchange between donor and acceptor vesicles. Furthermore, a preference of a gA monomer for the composition of one leaflet versus the other in the gA-aLUVs may require additional tests of the interleaflet gA localization and vesicle stability. The thermodynamic phase properties of the bilayer in the presence of gA (whether in dimeric or monomeric state) should also be considered. For example, we found that gA broadens and slightly lowers the main transition temperature of DMPC-d54 (Fig. S5), similar to previous reports for DMPC (55). This effect is likely to depend on the channel concentration in the membrane as well as the bilayer lipid composition and is likely to differ among proteins. A gel environment, for example, could affect not only the protein dynamics but also the efficiency of lipid exchange during the aLUV preparation protocol (see (28)).

Rates of lipid flip-flop measured with NMR

The slow rate of spontaneous lipid flip-flop that we measured in the chemically symmetric vesicles in the absence of gA is consistent with previous reports (14,56). Flip-flop kinetics in the compositionally asymmetric membranes, however, was significantly faster (Fig. 5). Because both POPC and DMPC have phosphocholine headgroups, this increase is likely due to differences in the chain lengths of the lipids (16 and 18 carbons for POPC and 14 carbons for DMPC) and the corresponding leaflet thicknesses (Table S4). This explanation is consistent with results from small-angle neutron scattering experiments showing a faster flip-flop rate in DMPC LUVs compared to POPC LUVs (56) and the corresponding free energy for flip-flop in the two bilayers, quantified with MD simulations (57).

Our results for the gA-mediated half time of lipid translocation in the POPC liposomes ($t_{1/2} \approx 64$ h at 22°C and a gA/lipid ratio of 1:40) are comparable to those of Fattal et al. who used the chain-labeled fluorescent lipid analog 1-oleoyl-2-[12-[(7-nitro-1,2,3-benzoxadiazol-4-yl)amino] dodecanoyl] phosphatidylcholine (NBD-PC) to determine a half time $t_{1/2} > 96$ h in POPC vesicles at room temperature and a gA/lipid ratio of 1:30 (14). This similarity is surprising in light of the different chemical structures of the acyl chains of NBD-PC relative to POPC and suggests that—in agreement with earlier experimental observations (58)—the nature of the lipid headgroup is the dominant factor in determining the flip-flop rate. Yet, the chain structure also has been shown to strongly affect flip-flop for lipids with multiple double bonds (59). In contrast, the reported kinetics of lipid translocation in the presence of gA in erythrocytes (24) and supported lipid bilayers (25) are much faster, likely because of the specific experimental conditions in the studies as mentioned in the Introduction.

The lipid flip-flop rates accessible to NMR measurements are limited by the time needed to perform a single experiment with the shift reagent. Depending on the type of instrument (i.e., the strength of the magnet) and sample concentration, one measurement in the absence of shift reagent, followed by 3 Pr^{3+} titrations (needed to obtain error bars, for example), could take anywhere from 15 min to 1 h. Thus, this technique can be used to measure only slower time-dependent translocation processes. However, because the lipid flip-flop rate would be expected to increase with increasing temperatures, systems with faster rates can be compared if incubated at lower temperatures (see also (60)). All samples in this study were incubated on the benchtop at an ambient temperature of ~22°C.

Mechanisms of gA-induced lipid scrambling

It has previously been proposed that the ability of gA to scramble lipid analogs is not due to bilayer perturbations induced by individual gA channels because of the following (23,24): 1) gA increases the translocation rate of lysophosphatidylcholine only at concentrations much higher than those in which gA performed its normal function as a conducting channel, but in which gA produces nonspecific solute leakage; and 2) formylation of gA's tryptophan residues, which prevents the clustering of gA, abolished the gA-catalyzed lyso-lipid scrambling. Instead, it was proposed that gA at gA/lipid mole fractions of 1:2000 or higher forms some sort of lateral aggregate(s) in the erythrocyte membrane that may be intermediates for the formation of hexagonal phases. The proposed clusters would induce transient defects in the bilayer with a subsequent formation of aqueous leaks that allow for the passage of molecules as large as choline and sucrose across the cell membrane as well as the translocation of lipid analogs (24). The proposed formation of gA clusters would depend on channel-bilayer hydrophobic mismatch because gA did not cause detectable aggregates in DMPC bilayers, in which there is minimal channel-bilayer hydrophobic mismatch (46) and little accumulation of stress in the membrane.

The lamellar SAXS form factors of POPC liposomes used in this study (Fig. 1 *A*) definitively exclude the presence of nonlamellar phases known to form at high gA concentrations under different experimental conditions (19). We can also exclude changes in the lateral association of gA in the asymmetric liposomes because aggregation to even as few as a 2-mer (two gA dimers) is expected to abrogate the liftoff effect of the gA 1-mer in the SAXS form factor, which is not seen in the experimental data (see Fig. 1; Supporting Materials and Methods). We further observe that gA broadens, but does not shift, the main transition temperature of the aLUVs (Fig. S6 *A*) as well as the sLUVs made of a binary mixture of DMPC-d54 and

POPC (Fig. S6 *B*). According to the model in (55), the lack of a shift is consistent with the gA exhibiting ideal mixing in both phases, though nonideal mixing would be expected at larger channel-bilayer hydrophobic mismatches.

In this context, our NMR and computational analysis further illuminates the importance of the frustration energy in the bilayer: at high channel densities, the bilayer thickness is not able to relax to its unperturbed state between the channels (Fig. 6), leading to bilayer-deformation-induced stress. This stress would increase the probability of transient clusters of bilayer-spanning gA channels (61–63), which could serve to decrease the energy barrier for lipid translocation and thereby increase the lipid flip-flop rate (64). The deviation of the gA-aLUVs at a gA/lipid ratio of 1:200 from the other samples in Fig. 6 *B* further suggests that at this lower gA mole fraction, the role of the frustration energy is different, resulting in a mechanistically distinct route for the observed gA effect on lipid flip-flop.

CONCLUSION

Applying, to our knowledge, new methodologies and protocols for preparing and characterizing asymmetric proteoliposomes to the system of gA channels, we have demonstrated the ability of gA to accelerate interleaflet lipid translocation in both chemically symmetric and asymmetric membranes. The mechanistic analysis of the results shows that the channel-induced bilayer deformation likely contributes to the rate of lipid flip-flop. The ability to characterize and quantify the interplay between TM proteins and their solvating lipid environment allows us to determine the properties of the protein-laden bilayers. If such properties are considered properly (e.g., with the type of methodology illustrated here), the mechanistic understanding of much more complex biomimetic systems becomes feasible and practical.

SUPPORTING MATERIAL

Supporting Materials and Methods, 12 figures, and six tables are available at http://www.biophysj.org/biophysj/supplemental/S0006-3495(19)30051-7.

AUTHOR CONTRIBUTIONS

M.D., F.A.H., H.W., G.W.F., and O.S.A. designed the research. M.D., F.A.H., R.R., R.L.S., and T.A.P. performed the experiments. M.D., F.A.H., D.M., and T.A.P. analyzed the experimental data. M.D. performed all MD simulations and computational analysis. M.D., F.A.H., D.M., J.K., G.W.F., H.W., and O.S.A. wrote the manuscript.

ACKNOWLEDGMENTS

We thank Haden Scott for technical assistance with CD measurements, Andrew Beaven for providing the MD force-field parameters for gA, and W. Clay Bracken for help with identifying the water suppression conditions for the NMR measurements at Weill Cornell Medical College.

This work was supported by National Science Foundation grant MCB-1817929 (to F.A.H.), National Institutes of Health grants P01 DA012408 (to H.W.) and R01 GM021342 (to O.S.A.), and by a grant from Natural Sciences and Engineering Research Council of Canada (funding reference number 2018-04841) (to D.M.). GC/MS, DSC, and DLS measurements were supported by the Biophysical Characterization Laboratory suite of the Shull Wollan Center at Oak Ridge National Laboratory. SAXS measurements were supported by Department of Energy scientific user facilities at Oak Ridge National Laboratory.

REFERENCES

1. Collins, M. D., and S. L. Keller. 2008. Tuning lipid mixtures to induce or suppress domain formation across leaflets of unsupported asymmetric bilayers. *Proc. Natl. Acad. Sci. USA.* 105:124–128.
2. Kiessling, V., C. Wan, and L. K. Tamm. 2009. Domain coupling in asymmetric lipid bilayers. *Biochim. Biophys. Acta.* 1788:64–71.
3. Perillo, V. L., D. A. Peñalva, …, S. S. Antollini. 2016. Transbilayer asymmetry and sphingomyelin composition modulate the preferential membrane partitioning of the nicotinic acetylcholine receptor in Lo domains. *Arch. Biochem. Biophys.* 591:76–86.
4. Vitrac, H., D. M. MacLean, …, W. Dowhan. 2015. Dynamic membrane protein topological switching upon changes in phospholipid environment. *Proc. Natl. Acad. Sci. USA.* 112:13874–13879.
5. Perlmutter, J. D., and J. N. Sachs. 2011. Interleaflet interaction and asymmetry in phase separated lipid bilayers: molecular dynamics simulations. *J. Am. Chem. Soc.* 133:6563–6577.
6. St. Clair, J. R., Q. Wang, …, E. London. 2017. Preparation and physical properties of asymmetric model membrane vesicles. *In* The Biophysics of Cell Membranes. R. Epand and J. M. Ruysschaert, eds. Springer, pp. 1–27.
7. Markones, M., C. Drechsler, …, S. Fiedler. 2018. Engineering asymmetric lipid vesicles: accurate and convenient control of the outer leaflet lipid composition. *Langmuir.* 34:1999–2005.
8. Takaoka, R., H. Kurosaki, …, M. Nakano. 2018. Formation of asymmetric vesicles via phospholipase D-mediated transphosphatidylation. *Biochim. Biophys. Acta. Biomembr.* 1860:245–249.
9. Contreras, F. X., L. Sánchez-Magraner, …, F. M. Goñi. 2010. Transbilayer (flip-flop) lipid motion and lipid scrambling in membranes. *FEBS Lett.* 584:1779–1786.
10. Sperotto, M. M., and A. Ferrarini. 2017. Spontaneous lipid flip-flop in membranes: a still unsettled picture from experiments and simulations. *In* The Biophysics of Cell Membranes. R. Epand and J. M. Ruysschaert, eds. Springer, pp. 29–60.
11. Pomorski, T. G., and A. K. Menon. 2016. Lipid somersaults: uncovering the mechanisms of protein-mediated lipid flipping. *Prog. Lipid Res.* 64:69–84.
12. Sebastian, T. T., R. D. Baldridge, …, T. R. Graham. 2012. Phospholipid flippases: building asymmetric membranes and transport vesicles. *Biochim. Biophys. Acta.* 1821:1068–1077.
13. Aye, I. L., A. T. Singh, and J. A. Keelan. 2009. Transport of lipids by ABC proteins: interactions and implications for cellular toxicity, viability and function. *Chem. Biol. Interact.* 180:327–339.
14. Fattal, E., S. Nir, …, F. C. Szoka, Jr. 1994. Pore-forming peptides induce rapid phospholipid flip-flop in membranes. *Biochemistry.* 33:6721–6731.
15. Tieleman, D. P., and S. J. Marrink. 2006. Lipids out of equilibrium: energetics of desorption and pore mediated flip-flop. *J. Am. Chem. Soc.* 128:12462–12467.
16. Ernst, O. P., and A. K. Menon. 2015. Phospholipid scrambling by rhodopsin. *Photochem. Photobiol. Sci.* 14:1922–1931.

17. Andersen, O. S., and R. E. Koeppe, II. 2007. Bilayer thickness and membrane protein function: an energetic perspective. *Annu. Rev. Biophys. Biomol. Struct.* 36:107–130.

18. de Kruijff, B., E. J. van Zoelen, and L. L. van Deenen. 1978. Glycophorin facilitates the transbilayer movement of phosphatidylcholine in vesicles. *Biochim. Biophys. Acta.* 509:537–542.

19. Tournois, H., J. Leunissen-Bijvelt, …, B. de Kruijff. 1987. Gramicidin-induced hexagonal HII phase formation in erythrocyte membranes. *Biochemistry.* 26:6613–6621.

20. Kol, M. A., A. I. de Kroon, …, B. de Kruijff. 2001. Membrane-spanning peptides induce phospholipid flop: a model for phospholipid translocation across the inner membrane of *E. coli*. *Biochemistry.* 40:10500–10506.

21. Kol, M. A., A. N. van Laak, …, B. de Kruijff. 2003. Phospholipid flop induced by transmembrane peptides in model membranes is modulated by lipid composition. *Biochemistry.* 42:231–237.

22. Anglin, T. C., K. L. Brown, and J. C. Conboy. 2009. Phospholipid flip-flop modulated by transmembrane peptides WALP and melittin. *J. Struct. Biol.* 168:37–52.

23. Killian, J. A. 1992. Gramicidin and gramicidin-lipid interactions. *Biochim. Biophys. Acta.* 1113:391–425.

24. Classen, J., C. W. Haest, …, B. Deuticke. 1987. Gramicidin-induced enhancement of transbilayer reorientation of lipids in the erythrocyte membrane. *Biochemistry.* 26:6604–6612.

25. Anglin, T. C., J. Liu, and J. C. Conboy. 2007. Facile lipid flip-flop in a phospholipid bilayer induced by gramicidin A measured by sum-frequency vibrational spectroscopy. *Biophys. J.* 92:L01–L03.

26. Marquardt, D., F. A. Heberle, …, G. Pabst. 2017. ^{1}H NMR shows slow phospholipid flip-flop in gel and fluid bilayers. *Langmuir.* 33:3731–3741.

27. Kucerka, N., J. Pencer, …, J. Katsaras. 2007. Curvature effect on the structure of phospholipid bilayers. *Langmuir.* 23:1292–1299.

28. Doktorova, M., F. A. Heberle, …, D. Marquardt. 2018. Preparation of asymmetric phospholipid vesicles for use as cell membrane models. *Nat. Protoc.* 13:2086–2101.

29. Ingólfsson, H. I., and O. S. Andersen. 2010. Screening for small molecules' bilayer-modifying potential using a gramicidin-based fluorescence assay. *Assay Drug Dev. Technol.* 8:427–436.

30. Heberle, F. A., D. Marquardt, …, G. Pabst. 2016. Subnanometer structure of an asymmetric model membrane: interleaflet coupling influences domain properties. *Langmuir.* 32:5195–5200.

31. Jo, S., T. Kim, …, W. Im. 2008. CHARMM-GUI: a web-based graphical user interface for CHARMM. *J. Comput. Chem.* 29:1859–1865.

32. Jo, S., J. B. Lim, …, W. Im. 2009. CHARMM-GUI membrane Builder for mixed bilayers and its application to yeast membranes. *Biophys. J.* 97:50–58.

33. Lee, J., X. Cheng, …, W. Im. 2016. CHARMM-GUI input generator for NAMD, GROMACS, AMBER, OpenMM, and CHARMM/OpenMM simulations using the CHARMM36 additive force field. *J. Chem. Theory Comput.* 12:405–413.

34. Doktorova, M., and H. Weinstein. 2018. Accurate in silico modeling of asymmetric bilayers based on biophysical principles. *Biophys. J.* 115:1638–1643.

35. Phillips, J. C., R. Braun, …, K. Schulten. 2005. Scalable molecular dynamics with NAMD. *J. Comput. Chem.* 26:1781–1802.

36. Klauda, J. B., V. Monje, …, W. Im. 2012. Improving the CHARMM force field for polyunsaturated fatty acid chains. *J. Phys. Chem. B.* 116:9424–9431.

37. Klauda, J. B., R. M. Venable, …, R. W. Pastor. 2010. Update of the CHARMM all-atom additive force field for lipids: validation on six lipid types. *J. Phys. Chem. B.* 114:7830–7843.

38. Beaven, A. H., A. M. Maer, …, W. Im. 2017. Gramicidin A channel formation induces local lipid redistribution I: experiment and simulation. *Biophys. J.* 112:1185–1197.

39. Heberle, F. A., J. Pan, …, J. Katsaras. 2012. Model-based approaches for the determination of lipid bilayer structure from small-angle neutron and X-ray scattering data. *Eur. Biophys. J.* 41:875–890.

40. Bystrov, V. F., and A. S. Arsenev. 1988. Diversity of the gramicidin A spatial structure: two-dimensional 1H NMR study in solution. *Tetrahedron.* 44:925–940.

41. Galbraith, T. P., and B. A. Wallace. 1999. Phospholipid chain length alters the equilibrium between pore and channel forms of gramicidin. *Faraday Discuss.* 11:159–164, discussion 225–246.

42. Perly, B., I. C. Smith, …, K. U. Ingold. 1985. Estimation of the location of natural alpha-tocopherol in lipid bilayers by 13C-NMR spectroscopy. *Biochim. Biophys. Acta.* 819:131–135.

43. Andersen, O. S., M. J. Bruno, …, R. E. Koeppe, II. 2007. Single-molecule methods for monitoring changes in bilayer elastic properties. *Methods Mol. Biol.* 400:543–570.

44. Lundbaek, J. A., S. A. Collingwood, …, O. S. Andersen. 2010. Lipid bilayer regulation of membrane protein function: gramicidin channels as molecular force probes. *J. R. Soc. Interface.* 7:373–395.

45. Katsaras, J., R. S. Prosser, …, J. H. Davis. 1992. Constant helical pitch of the gramicidin channel in phospholipid bilayers. *Biophys. J.* 61:827–830.

46. Harroun, T. A., W. T. Heller, …, H. W. Huang. 1999. Experimental evidence for hydrophobic matching and membrane-mediated interactions in lipid bilayers containing gramicidin. *Biophys. J.* 76:937–945.

47. Kučerka, N., M. P. Nieh, and J. Katsaras. 2011. Fluid phase lipid areas and bilayer thicknesses of commonly used phosphatidylcholines as a function of temperature. *Biochim. Biophys. Acta.* 1808:2761–2771.

48. Mondal, S., G. Khelashvili, …, H. Weinstein. 2011. Quantitative modeling of membrane deformations by multihelical membrane proteins: application to G-protein coupled receptors. *Biophys. J.* 101:2092–2101.

49. Lin, Q., and E. London. 2014. The influence of natural lipid asymmetry upon the conformation of a membrane-inserted protein (perfringolysin O). *J. Biol. Chem.* 289:5467–5478.

50. Hwang, W. L., M. Chen, …, H. Bayley. 2008. Asymmetric droplet interface bilayers. *J. Am. Chem. Soc.* 130:5878–5879.

51. Hussain, N. F., A. P. Siegel, …, C. A. Naumann. 2013. Bilayer asymmetry influences integrin sequestering in raft-mimicking lipid mixtures. *Biophys. J.* 104:2212–2221.

52. Vitrac, H., M. Bogdanov, and W. Dowhan. 2013. In vitro reconstitution of lipid-dependent dual topology and postassembly topological switching of a membrane protein. *Proc. Natl. Acad. Sci. USA.* 110:9338–9343.

53. Mobashery, N., C. Nielsen, and O. S. Andersen. 1997. The conformational preference of gramicidin channels is a function of lipid bilayer thickness. *FEBS Lett.* 412:15–20.

54. Lum, K., H. I. Ingólfsson, …, O. S. Andersen. 2017. Exchange of gramicidin between lipid bilayers: implications for the mechanism of channel formation. *Biophys. J.* 113:1757–1767.

55. Ivanova, V. P., I. M. Makarov, …, T. Heimburg. 2003. Analyzing heat capacity profiles of peptide-containing membranes: cluster formation of gramicidin A. *Biophys. J.* 84:2427–2439.

56. Nakano, M., M. Fukuda, …, T. Handa. 2009. Flip-flop of phospholipids in vesicles: kinetic analysis with time-resolved small-angle neutron scattering. *J. Phys. Chem. B.* 113:6745–6748.

57. Sapay, N., W. F. D. Bennett, and D. P. Tieleman. 2009. Thermodynamics of flip-flop and desorption for a systematic series of phosphatidylcholine lipids. *Soft Matter.* 5:3295–3302.

58. Homan, R., and H. J. Pownall. 1988. Transbilayer diffusion of phospholipids: dependence on headgroup structure and acyl chain length. *Biochim. Biophys. Acta.* 938:155–166.

59. Renooij, W., and L. M. Van Golde. 1977. The transposition of molecular classes of phosphatidylcholine across the rat erythrocyte

membrane and their exchange between the red cell membrane and plasma lipoproteins. *Biochim. Biophys. Acta.* 470:465–474.

60. Wolfenden, R., and M. J. Snider. 2001. The depth of chemical time and the power of enzymes as catalysts. *Acc. Chem. Res.* 34:938–945.

61. Goforth, R. L., A. K. Chi, …, O. S. Andersen. 2003. Hydrophobic coupling of lipid bilayer energetics to channel function. *J. Gen. Physiol.* 121:477–493.

62. Rokitskaya, T. I., E. A. Kotova, and Y. N. Antonenko. 2003. Tandem gramicidin channels cross-linked by streptavidin. *J. Gen. Physiol.* 121:463–476.

63. Lewis, B. A., and D. M. Engelman. 1983. Bacteriorhodopsin remains dispersed in fluid phospholipid bilayers over a wide range of bilayer thicknesses. *J. Mol. Biol.* 166:203–210.

64. Gurtovenko, A. A., and I. Vattulainen. 2007. Molecular mechanism for lipid flip-flops. *J. Phys. Chem. B.* 111:13554–13559.

Biophysical Journal, Volume *116*

Supplemental Information

Gramicidin Increases Lipid Flip-Flop in Symmetric and Asymmetric Lipid Vesicles

Milka Doktorova, Frederick A. Heberle, Drew Marquardt, Radda Rusinova, R. Lea Sanford, Thasin A. Peyear, John Katsaras, Gerald W. Feigenson, Harel Weinstein, and Olaf S. Andersen

Table S1. Asymmetric samples examined in each experiment. Shown are the donor and acceptor lipid pairs; the corresponding experiments (Exp.); gA-to-lipid ratio (gA:L); nominal donor:acceptor ratio (D:A); mole fraction of donor in the final asymmetric sample determined from GC (χ_{don}); and the area fraction of the shifted choline resonance peak measured with NMR after sample preparation ($C_{\mathrm{out}}(t=0)$) indicating the initial fraction of donor lipid on the outer leaflet of the vesicles.

Donor	Acceptor	Exp.	gA:L	D:A	χ_{don}	$C_{\mathrm{out}}(t=0)$
POPC-d31	POPC	GBFA	1:20000	2	0.32	-
	POPC-d13	SAXS	1:40	3	0.4	-
		NMR	0	2	0.34	0.87 (0.03)
			1:40	2	0.33	0.76 (0.02)
			1:100	3	0.38	0.76 (0.02)
DMPC-d54	POPC	GBFA	1:20000	2	0.35	-
		CD	1:40	3	0.45	-
		DSC	0	3	0.42	-
			1:40	3	0.4	-
	POPC-d13	NMR	0	3	0.43	0.85 (0.02)
			1:40	3	0.4	0.78 (0.01)
			1:200	3	0.42	0.88 (0.01)

Table S2. Representative vesicle sizes measured with dynamic light scattering (DLS). Shown are the acceptor and donor lipid composition, and the diameter (D) and polydispersity index (PI) of the symmetric acceptor vesicles and the final asymmetric vesicles.

acceptor	donor	symmetric acceptor LUVs		final asymmetric LUVs	
		D [nm]	PI	D [nm]	PI
POPC-d13/gA (1:40)	POPC-d31	146.6	0.072	153.9	0.123
POPC-d13/gA (1:100)		129.9	0.005	129.2	0.118
POPC-d13	DMPC-d54	122.8	0.108	126.9	0.151
POPC/gA (1:40)		137.0	0.101	136.8	0.216
POPC/gA (1:20,000)		122.5	0.109	128.0	0.131

Table S3. Effect of Pr^{3+} on bilayer properties. The rates of ANTS quenching by TI^{+} in symmetric LUVs composed of DEPC (di22:1 PC) and gA at gA:lipid ratio of 1:2096, and mixed with different amounts of the shift reagent Pr^{3+}. (In the NMR experiments described in the text the sample gets exposed to at most 0.1 mM Pr^{3+} after the three Pr^{3+} titrations, which corresponds to a Pr^{3+}:lipid ratio of ~1:7.) The ANTS quenching rates are representative of bilayer compressibility with an increase and decrease indicating softening and stiffening of the bilayer, respectively. Relative to the sample without Pr^{3+}, no significant changes in the rate were observed, confirming that the shift reagent does not alter bilayer properties.

Composition	Pr^{3+}:lipid ratio	Average Rate (s^{-1})	Stdev
gA	0	24.2	1.7
gA + 3 mM Pr^{3+}	60	21.9	2.3
gA + 10 mM Pr^{3+}	200	25.6	3.4

Table S4. Simulated bilayers without gramicidin. Shown are the total simulation time and the last equilibrated portion of each trajectory used for analysis. Equilibration was assessed from convergence of the area per lipid quantified with the algorithm from [1]. Also shown for each leaflet are the average area per lipid, A_{lip} (equal to the lateral area of the simulation box divided by the number of lipids in the leaflet); the area compressibility modulus, K_A (calculated from local thickness fluctuations as described in [2]); the bending rigidity modulus, κ_C (calculated from local splay fluctuations as described in [3, 4]); and the average leaflet thickness (calculated as described in Section S.2). Errors are shown in parentheses. The errors on A_{lip} are standard errors calculated from consecutive time blocks of length equal to the effective number of samples [1]. Errors on K_A and κ_C were calculated as described in Refs. [2] and [3, 4], respectively.

Bilayer	Leaf	Simulation time [ns]		A_{lip} [A^2]	K_A† [mN/m]	κ_C† [k_BT]	d_0† [A]
		analysis	total				
§POPC	Top	183	226	64.3 (0.2)	236 (26)	12.9 (0.5)	17.8
	Bot				186 (28)	12.4 (0.6)	17.7
§DMPC/POPC 0.75/0.25	Top	738	738	61.4 (0.1)	282 (24)	15.4 (0.6)	16.8
	Bot				244 (38)	14.8 (0.5)	16.8
§DMPC/POPC 0.10/0.90	Top	471	471	63.8 (0.1)	238 (22)	12.8 (0.6)	17.7
	Bot				188 (32)	11.7 (0.4)	17.7
Asymmetric DMPC/POPC	Top	280	445	61.4 (0.1)	286 (32)	15 (0.5)	16.8
	Bot			63.8 (0.1)	224 (26)	12.5 (0.5)	17.7

§ Bilayer systems taken from [5].

† For the symmetric bilayers, the corresponding average leaflet quantity was used in the membrane deformations analysis described in Section S3.

Table S5. Structural parameters for POPC at 25°C obtained from modeling SAXS data.

Parameter	Symbol [units]	Value	Literature value[a]
Total lipid volume	V_L [Å^3]	1249.0	1251.5[b]
Headgroup volume	V_{HL} [Å^3]	331[b]	331[b]
Area per lipid	A_L [Å^2]	63.9	63.5
Bilayer (Luzzati) thickness	D_B [Å]	39.1	39.5
Phosphate-phosphate distance	D_{HH} [Å]	35.8	37.0
Hydrocarbon thickness	$2D_C$ [Å]	28.7	29.0

[a]Ref. [6] [b]fixed parameter

Table S6. Parameters for modeling the gA transmembrane dimer and associated water in Monte Carlo simulations of small-angle scattering curves.

Parameter	Symbol [units]	Value
Volume of gA dimer and associated water	V_{gA} [Å^3]	5456
Area of gA domain	a_{cyl} [Å^2]	221
Radius of gA domain	r_{cyl} [Å]	8.4
Thickness of gA domain	t_{cyl} [Å]	24.7
Number of associated waters	N_w	10
Total number of electrons in gA domain	N_{e^-}	2118
Electron density of gA domain	ρ_{gA} [e$^-$ Å^{-3}]	0.388

Figures

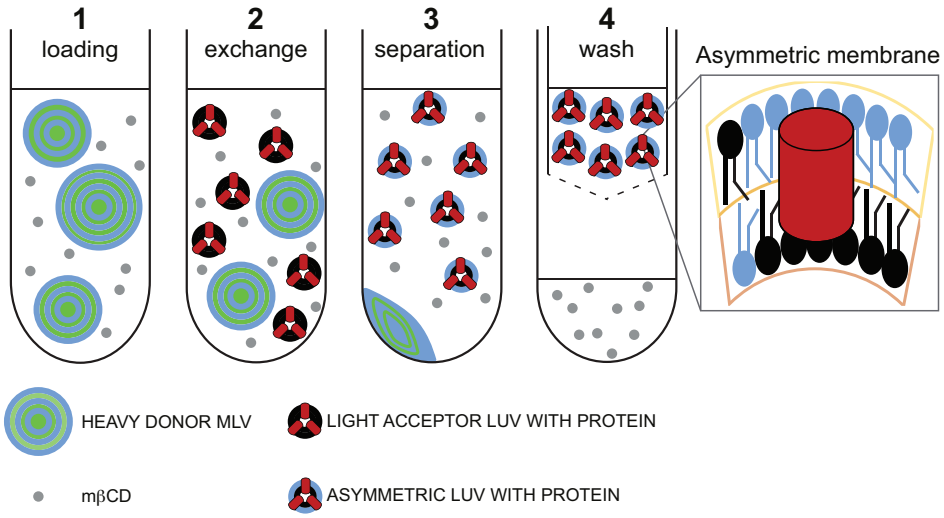

Figure S1. Schematic illustration of the protocol for preparation of asymmetric proteoliposomes. Step 1, MLVs of donor lipid are incubated with MβCD for 2 h at room temperature with gentle stirring. Step 2, extruded symmetric LUVs with gramicidin are added to the donor lipid/MβCD solution, and the acceptor/donor/MβCD mixture is incubated at room temperature with gentle stirring. Step 3, donor MLVs are separated from the asymmetric vesicles and cyclodextrin after an 8-fold dilution with H_2O and centrifugation at 20,000 x g for 30 min. Step 4, cyclodextrin is removed with centrifugal filter devices, and the sample is washed at least 3 times with water (or another appropriate solvent). The final asymmetric proteoliposomes are recovered from the retentate. The schematic is adapted from Ref. [7].

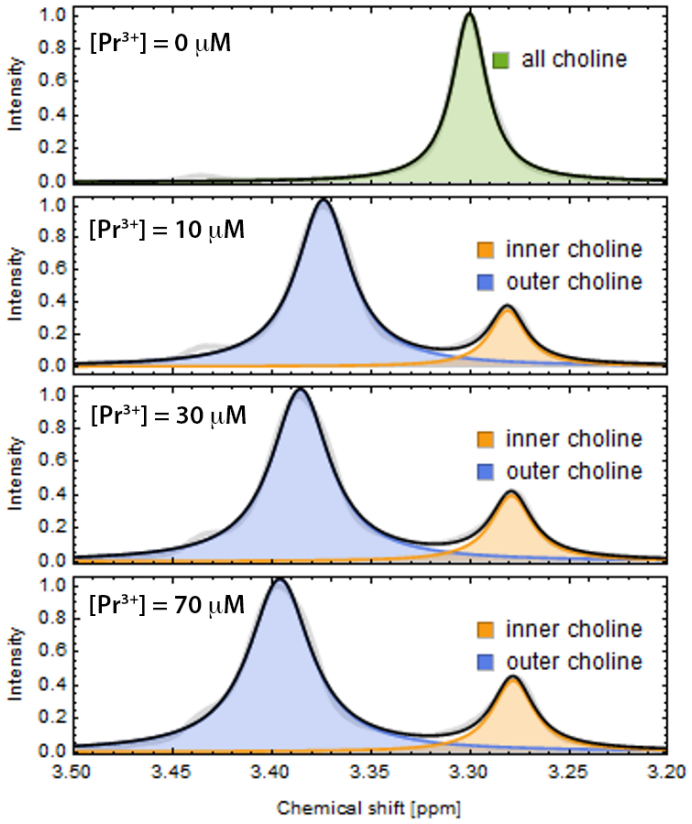

Figure S2. Representative ^{1}H NMR spectra of a gA-aLUV sample prepared with POPC-d13 acceptor and DPMC-d54 donor vesicles. In each panel, the solid gray line is the experimentally measured spectrum and the solid black line is the fitted sum of one or two Lorentzians (shown individually as shaded regions). *Upper panel*, prior to addition of the shift reagent Pr^{3+}, a single peak is observed corresponding to the headgroup-protiated donor lipid located in both leaflets. Lower three panels, external addition of increasing amounts of Pr^{3+} to the sample results in a gradual downfield shift of the outer leaflet donor lipid (blue shading). Donor lipid residing in the inner leaflet (orange shading) is essentially protected from the shift reagent. The peak areas are proportional to the amount of lipid in each environment.

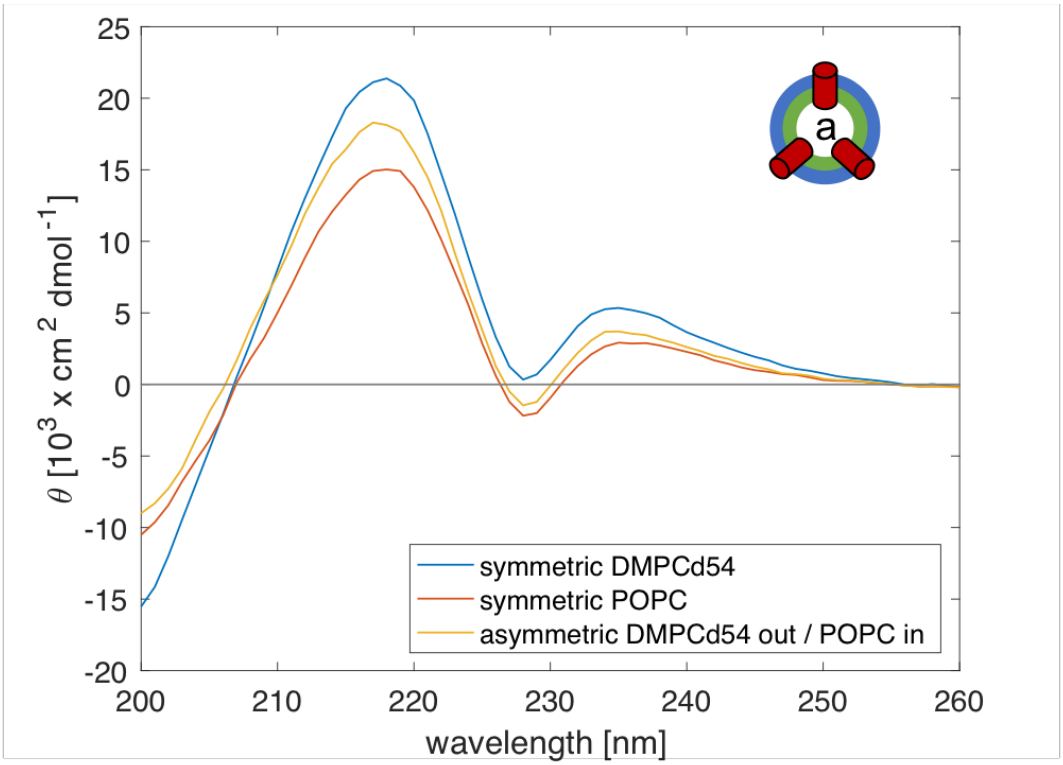

Figure S3. Circular dichroism spectra of gA-containing DMPC-d54 (blue) and POPC (red) sLUVs, and compositionally asymmetric LUVs composed of DMPC-d54 and POPC (yellow). All liposomes were prepared at a gA:lipid ratio of 1:40, and all measurements were performed at 25°C.

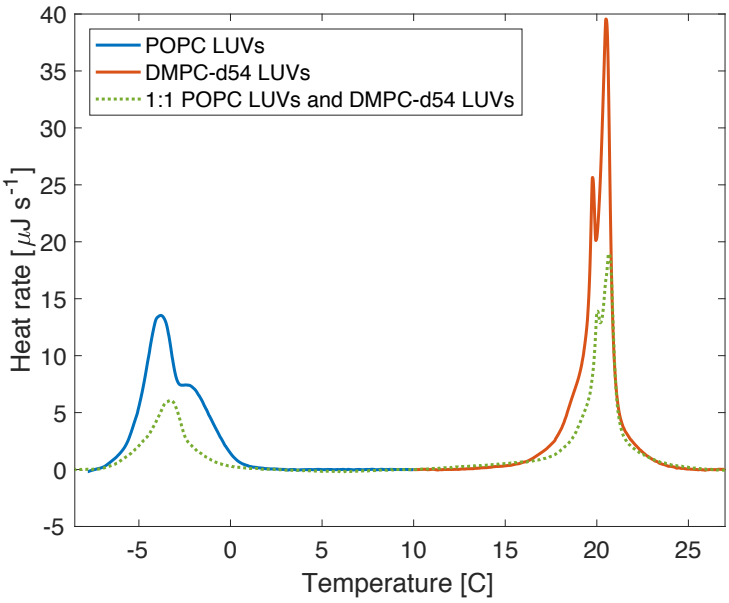

Figure S4. DSC thermograms for POPC LUVs (blue), DMPC-d54 LUVs (red) and a 1:1 mixture of POPC LUVs and DMPC-d54 LUVs (dotted green).

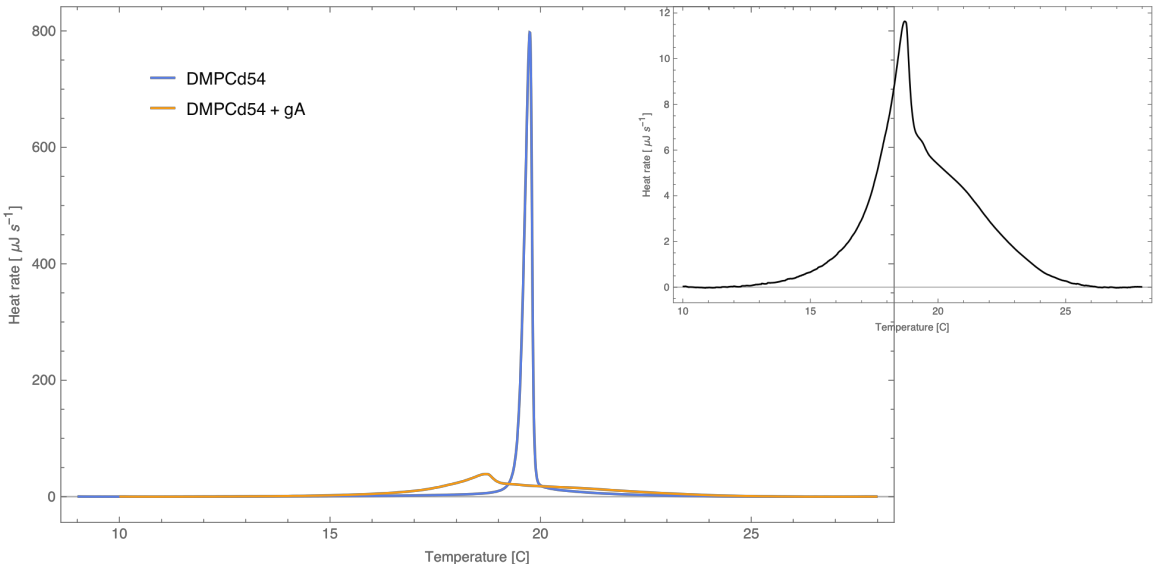

Figure S5. DSC thermograms for DMPCd54 symmetric vesicles without (blue) and with (orange) gA at gA:lipid ratio of 1:40. The inset shows a zoomed in version of the gA-sLUV thermogram. The presence of gA broadens the melting transition of the sample and slightly decreases it.

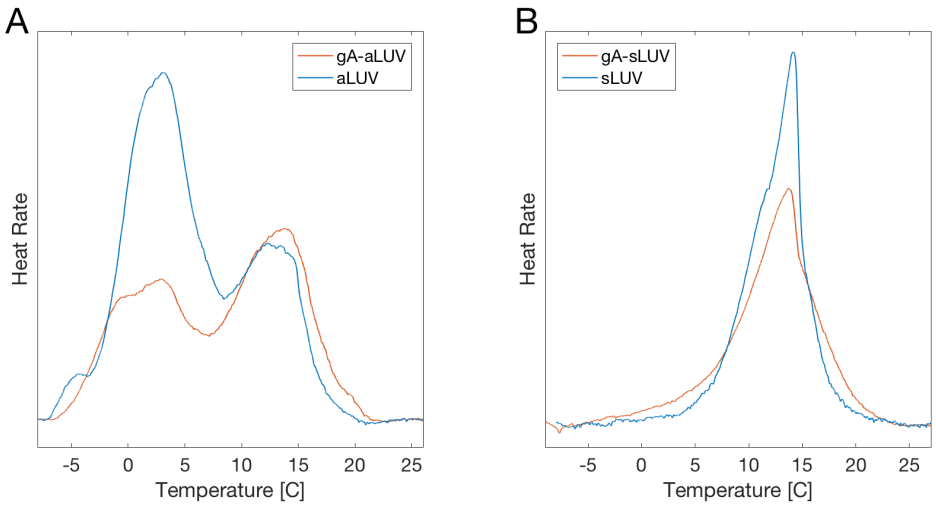

Figure S6. DSC thermograms for asymmetric (A) and symmetric vesicles (B) without and with gramicidin (at gA:lipid ratio of 1:40). The data in (A) is taken from Fig. 3 in the main text. The data in (B) is for vesicles made of DMPC-d54/POPC 75/25 mol%, a composition similar to that of the outer leaflet of the asymmetric vesicles in (A).

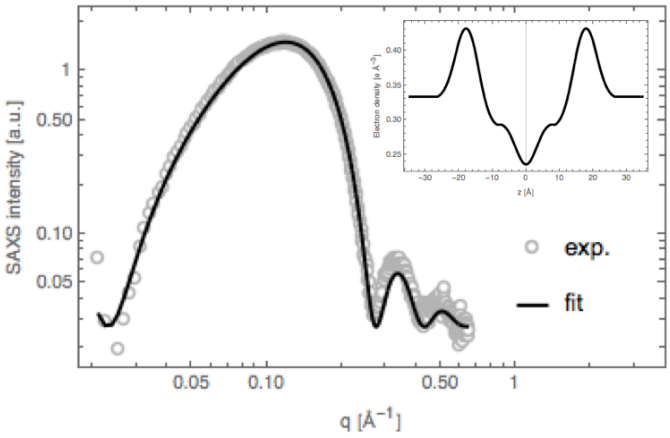

Figure S7. SAXS analysis of POPC data at 25°C. Experimental data (open circles) and fit (solid line) to a model of the lipid matter density distribution along the bilayer normal. The electron density profile corresponding to the best fit is shown in the inset.

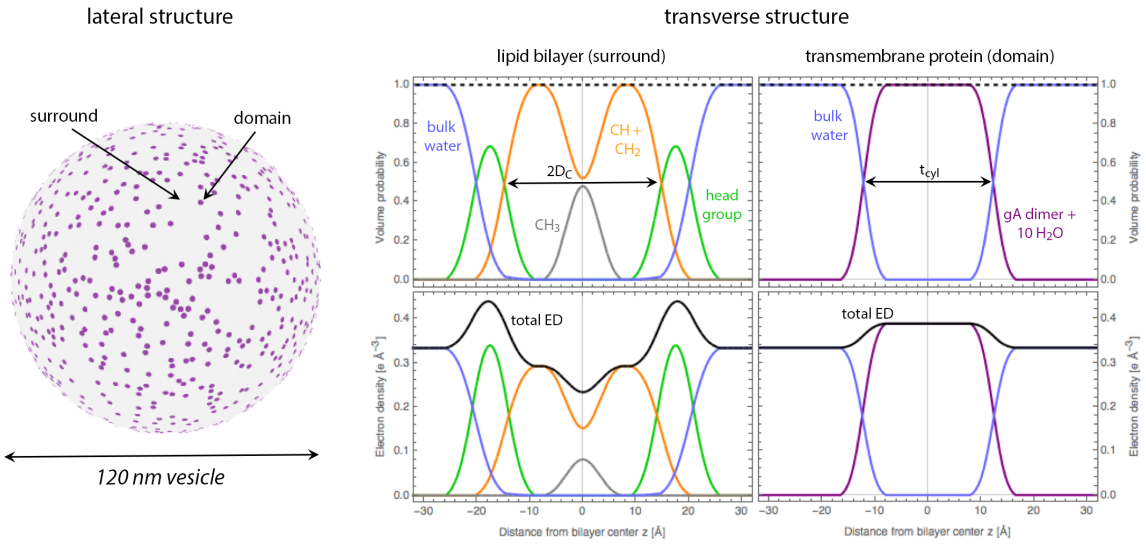

Figure S8. Schematic illustration of Monte Carlo scattering analysis. The MC analysis considers both lateral (i.e., in-plane) and transverse variation in the electron density within the proteoliposome. *Left*, the lateral structure corresponds to cylindrical gA (transmembrane dimer) domains randomly dispersed in the surrounding continuous POPC lipid bilayer. *Right*, the transverse structure of the lipid bilayer is given by the POPC volume probability profile, while that of the gA domain is given by a cylinder of uniform volume probability smoothed by convolution with a 2.0 Å-width Gaussian to mimic the effects of thermal disorder (upper panels). The corresponding total electron density (ED) profiles (black curves in lower panels) are inputs to the simulation. See Section S.4 for more details.

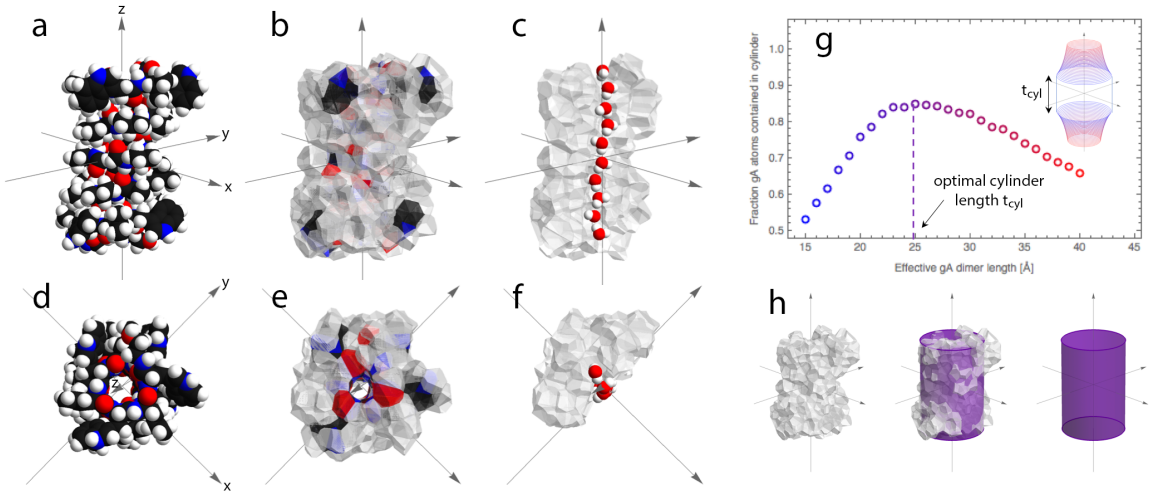

Figure S9. Determination of gramicidin channel structural parameters for Monte Carlo scattering simulations. (a) Space filling model of a gramicidin-A (gA) transmembrane dimer in a POPC bilayer from a molecular dynamics simulation, with CPK coloring (carbon is black, hydrogen is white, nitrogen is blue, oxygen is red). The z direction is normal to the (x,y) plane of the lipid bilayer. (b) A 3D Voronoi tessellation of the system yields one cell per atom, from which atomic volumes of gA and associated waters are obtained. (c) Cross-section of the 3D Voronoi representation of gA with the +x atoms removed to show the central cavity occupied by 10 water molecules (shown in space filling representation). (d), (e), and (f) are 90° rotations of panels a, b, and c, respectively, providing a view that looks down on the gA dimer from above the membrane. The water atoms are removed in panels d and e to show the central cavity. (g) Given the fixed gA+water channel volume V_{gA} obtained from the Voronoi analysis, a cylindrical representation of gA was found by maximizing the number of gA atoms enclosed in a cylinder of length t_{cyl} and area $a_{cyl} = V_{gA}/t_{cyl}$. The inset shows a graphical representation of all cylindrical volumes tested, color coded to the data points. (h) The optimal effective cylinder superimposed on the 3D Voronoi representation of gA. See Section S.4 for more details.

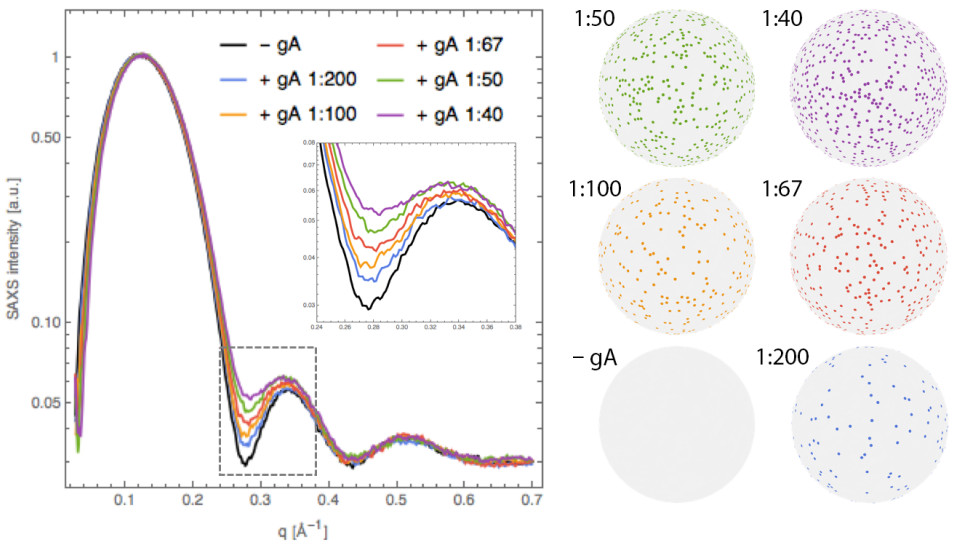

Figure S10. Effect of increasing gA concentration on simulated SAXS data. *Left*, increasing the bilayer concentration of gA up to a protein:lipid ratio of 1:40 systematically increases the intensity at the minimum between the first and second scattering lobes, shown in an expanded view in the inset. *Right*, Monte Carlo simulations snapshots corresponding to different gA:lipid ratios. See Section S.4 for more details.

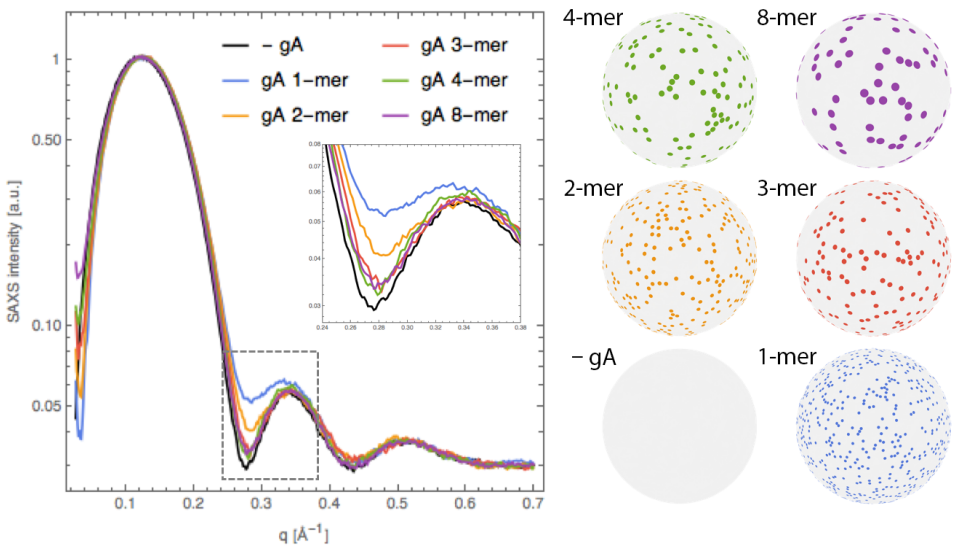

Figure S11. Effect of lateral gA association on simulated SAXS data. *Left*, lateral oligomerization of transmembrane gA dimers decreases the intensity at the minimum between the first and second scattering lobes, shown in an expanded view in the inset. A fixed gA:lipid ratio of 1:40 was used in all simulations. *Right*, Monte Carlo simulations snapshots corresponding to different oligomerization states. See Section S.4 for more details.

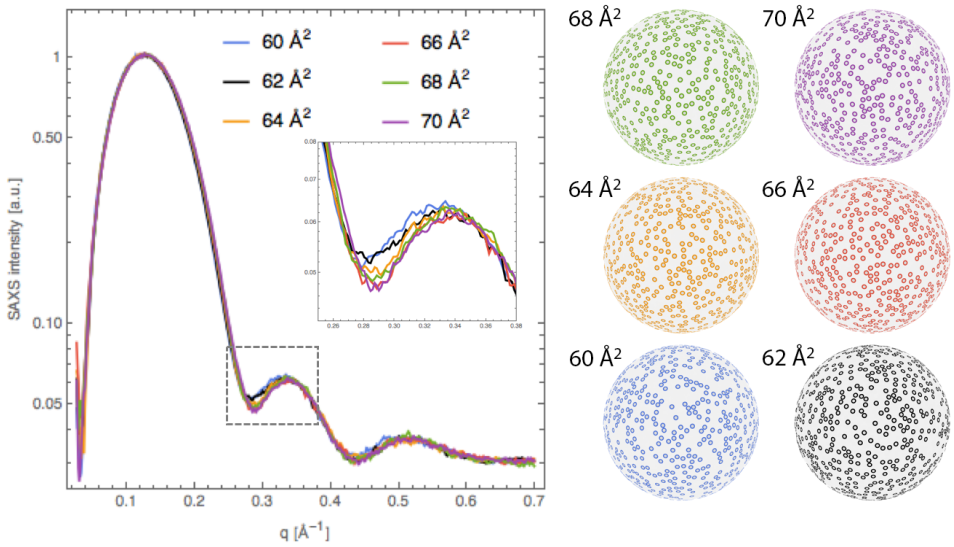

Figure S12. Effect of gA-induced lipid perturbation on simulated SAXS data. *Left*, bilayer thinning (i.e., increased area per lipid) of the first shell of 14 lipids surrounding a gA transmembrane dimer causes a slight decrease in the intensity at the minimum between the first and second scattering lobes, and a slight shift of the minimum to higher q, as shown in an expanded view in the inset. A fixed gA:lipid ratio of 1:40 and a bulk (unperturbed) area per lipid of 62.0 Å^2 were used in all simulations. *Right*, Monte Carlo simulations snapshots showing the first lipid shell surrounding the protein in a color that corresponds to the SAXS curves on the left. See Section S.4 for more details.

S.1. Simulation details. Table S4 lists all simulated bilayer systems without gramicidin. As indicated, the symmetric bilayers were taken from [5]. The asymmetric bilayer was simulated with the same simulation parameters as the symmetric ones: a 10-12 Å cutoff with NAMD's *vdwForceSwitchng* option turned on for Van der Waals and electrostatic interactions; Particle Mesh Ewald for long-range electrostatics, with grid spacing of 1 Å; Langevin thermostat set to maintain temperature at 25°C and a Nose-Hoover barostat with Langevin dynamics set to maintain pressure at 1 atm with a period of 200 fs and delay of 50 fs; and a time-step of 2 fs with fixed hydrogen bonds (i.e. *rigidbonds* option set to *all*).

The two gA-containing bilayer systems (one gA channel embedded into the symmetric POPC or asymmetric DMPC/POPC membrane as described in the text) were simulated with the same simulation parameters as outlined above.

S.2. Analysis of leaflet thickness from MD simulations. Local leaflet thicknesses were calculated with a modified version of VMD's MEMBPLUGIN tool for membrane thickness [8] as described in [2]. Briefly, the heights h of all heavy atoms on the lipid acyl chains, including the phosphate, were calculated at different grid points on the leaflet surface by interpolation on their z coordinates as follows:

$$h_{\varsigma,(x,y)} = \frac{\sum_i \frac{z_{\varsigma,i}}{d_{i,(x,y)}^2}}{\sum_i \frac{1}{d_{i,(x,y)}^2}}, \tag{S1}$$

where ς denotes the atom type (e.g. phosphate, C1 atom on the sn-1 chain, C2 atom on the sn-2 chain, etc.), x and y are the two-dimensional coordinates of the grid point, the summations are over all lipid atoms of type ς in the leaflet with $z_{\varsigma,i}$ being the z-coordinate of atom i and $d_{i,(x,y)}$ denoting the 2D distance between atom i and the grid point at (x, y). Once all heights have been calculated, the leaflet thickness τ at each grid point was simply the distance between the local height of the phosphate atom and the local height of the lowest-situated atom type at the grid point:

$$\tau_{P,(x,y)} = h_{P,(x,y)} - \min h_{(x,y)}. \tag{S2}$$

The average leaflet thickness d_0 in Table S4 is the space- and time-averaged local thickness τ_P in the leaflet.

S.3 Analysis of membrane deformation. The membrane deformation profile around a single gA channel was calculated by combining information from the simulation trajectories with the CTMD formalism in which the free energy of membrane deformation ΔG_{def} is expressed in terms of the area compressibility (K_A) and bending rigidity (κ_C) moduli of the lipid environment:

$$\Delta G_{\text{def}} = \frac{1}{2}\int_{\Omega} \left\{ K_a \left(\frac{u}{d_0}\right)^2 + \kappa_C \left(\frac{\partial^2 u}{\partial x^2} + \frac{\partial^2 u}{\partial y^2} - c_0\right)^2 - \kappa_C c_0^2 \right\} d\Omega. \tag{S3}$$

In the space integral in Eq. S3, $u = d - d_0$ is deviation from the equilibrium thickness and c_0 is spontaneous curvature. Generally, ΔG_{def} is calculated directly for the whole membrane and

used to obtain the optimal membrane deformation profile, i.e. the optimal u that minimizes ΔG_{def} subject to a number of boundary conditions.

Because the two membrane leaflets may deform in a different way around gA (especially in the case of an asymmetric membrane), here we treat each leaflet separately. Thus, if L denotes one leaflet (top or bottom) and $\Delta G_{\text{def}}^{L}$ is the corresponding free energy, then:

$$\Delta G_{\text{def}}^{L} = \frac{1}{2}\int_{\Omega} \left\{ K_a^L \left(\frac{u}{d_0}\right)^2 + \kappa_C^L \left(\frac{\partial^2 u}{\partial x^2} + \frac{\partial^2 u}{\partial y^2} - c_0\right)^2 - \kappa_C^L c_0^2 \right\} d\Omega, \qquad \text{(S4)}$$

where all mechanical constants, u, d_0 and c_0 represent the per leaflet quantities. Eq. S4 is used to obtain an optimal deformation profile for each leaflet L (as described in detail below) and the membrane deformation profile is then the sum of the deformation profiles of the two bilayer leaflets. In the procedure, the input from the MD simulations consists of (1) the mechanical constants (K_a^L and κ_C^L) and d_0 calculated from the bilayer-only trajectories as described in Section S.2 and listed in Table S4; and (2) the leaflet thickness at the gA-lipid boundary which is calculated from the gA containing trajectories as descried below and appears as one of the boundary conditions in the energy minimization procedure.

Thus, the following protocol, inspired by the methodology in [9], was used to calculate the optimal deformation profile for a leaflet L:

1. Identify the gA-lipid boundary in the leaflet and calculate the leaflet thickness at this boundary as described in the main text.
2. Solve the following boundary value problem:

$$\kappa_C^L \nabla^4 u + \left(\frac{K_a^L}{d_0^2}\right) u = 0 \qquad \text{where} \qquad \nabla^2 = \frac{\partial^2}{\partial x^2} + \frac{\partial^2}{\partial y^2} \qquad \text{(S5)}$$

subject to the boundary conditions:

$$u|_{\Gamma_{out}} = 0 \qquad \nabla u|_{\Gamma_{out}} = 0 \qquad u|_{\Gamma_{in}} = u_0(x,y) \qquad \nabla^2 u|_{\Gamma_{in}} = v_0(x,y) \qquad \text{(S6)}$$

where Γ_{out} and Γ_{in} denote the bulk and the protein-lipid interface respectively, and u_0 and v_0 are the deviation from d_0 and the curvature at the gA-lipid boundary accordingly. Both u_0 and v_0 can be non-uniform around the protein and are thus functions of x and y. $u_0(x,y)$ is calculated directly from the gA simulations by subtracting d_0 from the corresponding leaflet thickness at (x,y), while κ_C^L and K_a^L are calculated from the bilayer-only trajectories as described in the caption of Table S4.

v_0 is obtained through a self-consistent optimization procedure that aims to globally minimize $\Delta G_{\text{def}}^{L}$ by following a slightly modified version of the approach in [9]. In short, every (x,y) point on the gA-lipid boundary is first expressed as a function of an angle θ relative to the center of gA. Then $v_0(\theta)$ is expressed as a Fourier series truncated up to 7$^{\text{th}}$ order:

$$v_0(\theta) \sim \sum_{n=0}^{7} (a_n \cos n\theta + b_n \sin n\theta) \qquad \text{(S7)}$$

and is thus parameterized by only 15 parameters (a_0 through a_7 and b_1 through b_7). The 15 parameters are first chosen at random, then optimized using a quasi-Newton method for unconstrained minimization (the *fminunc* function in MATLAB) to find the minimum $\Delta G_{\mathrm{def}}^{L}$. For each set of parameters, $\Delta G_{\mathrm{def}}^{L}$ is obtained by:
(1) calculating $v_0(\theta)$ with Eq. S7,
(2) solving Eq. S5 for u subject to the four boundary conditions in Eq. S6 (which yield a unique solution), and
(3) using the resulting deformation profile u to get $\Delta G_{\mathrm{def}}^{L}$ with Eq. S4.
Eq. S5 is solved by using the 5-point stencil method (the 5-point finite difference approximation of the Laplacian operator) in two dimensions and expressing the problem in the form $Au = b$ where A is a nonsingular matrix, b is a vector and thus the solution can be computed as $u = A\backslash b$.

S.4. Analysis of SAXS data

S.4.1. Overview

In a small-angle scattering experiment, the scattering pattern at the detector is related to spatial and temporal variation in the distribution of matter on length scales of ~ 1–100 nm. More specifically, the distribution of scattering centers—electron density (ED) and neutron scattering length density (NSLD) for X-ray and neutron radiation, respectively—within the illuminated sample volume determine the coherent scattering intensity as a function of momentum transfer vector q. In a lipid bilayer, the different chemical makeup of lipid headgroups compared to their hydrocarbon chains results in a large variation in ED in the transverse direction along the bilayer normal (here referred to as the "z" direction) which results in characteristic lobes of scattering intensity vs. q (Fig. S7). In contrast, at any given z position there is much less ED variation in the (x,y) direction parallel to the plane of the bilayer. For this special case of a laterally homogeneous bilayer, the observed intensity $I(q)$ is dominated by scattering that arises from transverse variation in electron density.[1] To a very good approximation, $I(q)$ is then mathematically related to the real-space ED profile $\rho(z)$ by a simple one-dimensional Fourier transform.

The *homogeneous bilayer approximation* described above enables the prediction of X-ray (or neutron) scattering intensity given knowledge of the lipid matter density distribution across the bilayer. Conversely (and more commonly) it enables the determination of real-space structural parameters such as area per lipid and bilayer thickness from experimental scattering data when fitted with a suitable model. Fig. S7 shows the analysis of SAXS data from POPC unilamellar vesicles at 25°C using a typical transverse matter density model with distinct layers for the lipid headgroup, the combined hydrocarbon CH_2 and CH moieties, and the terminal CH_3 groups [10]. The best-fit curve produced by the model (solid black line) faithfully reproduces the experimental data (open circles), and the best-fit

[1] For spherical bilayered vesicles such as the unilamellar liposomes used in this study, the terms *transverse* and *lateral* should be replaced with *radial* and *angular*. We nevertheless use transverse and lateral instead as these terms are far more common in the literature of lipid bilayers.

parameters (Table S5) are in excellent agreement with literature values [6], demonstrating the robustness of scattering data and analysis.

Many single-component bilayers in the fluid phase have now been analyzed within the homogeneous bilayer approximation using models of varying degree of complexity [11, 12]. However, for multicomponent mixtures that exhibit substantial in-plane variation in scattering density, the homogeneous bilayer approximation is no longer valid and can fail to reproduce features in scattering data. Here, our motivation for employing a more sophisticated model that properly accounts for lateral ED variation is the enhanced scattering intensity seen at the minimum between the first two lobes of SAXS intensity in gA-containing liposomes (Fig. 1A in the main text). This feature cannot be accounted for within the homogeneous bilayer approximation, which predicts zero coherent scattering intensity at these minima for symmetric bilayers. As we will show now (and to our knowledge, for the first time), the liftoff observed in the SAXS data is in fact a hallmark of a transmembrane protein embedded in a lipid bilayer.

S.4.2. Methodology

We have previously used two different (but essentially equivalent) approaches to modeling small-angle scattering data from laterally heterogeneous bilayers. A purely analytical solution is based on a spherical harmonic expansion of the scattering potential, which separates the scattering form factor into orthogonal terms for the radial and angular scattering length density variation [13]. A simulation approach based on Monte Carlo (MC) sampling of the real-space distribution of scattering length density yields identical results to the analytical solution for the same underlying geometrical model of the bilayer [13]. Although these methods were developed specifically for the study of lipid phase separation using small-angle neutron scattering [14], the concepts apply equally well to the case of proteins embedded in lipid bilayers, as we will now show.

As mentioned previously, the standard analysis for small-angle scattering data from lipid bilayers is to model the real-space transverse scattering length density profile (in the case of SAXS data, the ED profile). This approach is inappropriate for laterally heterogeneous bilayers as it explicitly averages the in-plane structure and thus fails to capture coherent scattering arising from non-random lipid mixing or the presence of adsorbed or inserted proteins. There are two reasons why the homogeneous bilayer approximation is not valid for our experimental system: (1) the gA transmembrane dimer has a markedly different transverse ED profile than the lipid as shown in Fig. S8, resulting in a large contrast between protein and lipid and consequently a non-negligible contribution from the lateral/angular form factor; (2) the protein inclusion may perturb the local bilayer structure, resulting in additional lateral complexity. We chose to use the MC approach rather than the purely analytical solution primarily because it is relatively easy to simulate complicated geometries (such as shells of perturbed lipid) that are beyond the capabilities of the existing analytical framework.

The MC simulations, described in detail previously for the case of coexisting lipid phases [13, 14] and summarized schematically in Fig. S8, consider two environments within a unilamellar vesicle. Here, these are the gA transmembrane domains and the continuous

lipid bilayer that surrounds them. Each of these environments has a different transverse ED profile as shown in Fig. S8. We now briefly describe the different inputs to the simulations.

Transverse structure of the lipid bilayer. The ED profile obtained from fitting the POPC data in the absence of gA (Fig. S7 inset) was used as the ED profile of the continuous lipid bilayer except where noted below.

Transverse structure of the protein domain. We modeled the transverse ED profile of a gA transmembrane dimer as follows. The molecular volume of a gA dimer embedded in a POPC bilayer was determined from a 3D Voronoi tessellation of a single frame of an MD simulation as shown in Fig. S9. The Voronoi tessellation divides all atoms in the simulation box into individual 3D cells, from which effective atomic volumes are easily calculated. The total gA transmembrane dimer volume V_{gA} was calculated as the sum of the individual volumes of all atomic cells of the gA dimer, along with those of the ten water atoms lining the central cavity (Fig. S9*a-f*). An equivalent cylinder of identical volume was found by optimizing the length t_{cyl} and area a_{cyl} (where $V_{gA} = V_{cyl} = t_{cyl}a_{cyl}$) such that the resulting cylinder enclosed the largest fraction of gA atoms (Fig. S9*h*); the optimal cylinder (shown graphically in Fig. S9*g*) had a length of 24.7 Å and an area of 221 Å^2. The electron density ρ_{GA} of the gA domain was calculated as the total number of electrons in all atoms of the gA dimer and ten central waters, N_e–, divided by the gA volume V_{gA}, i.e. $\rho_{gA} = N_e-/V_{gA}$. The step ED profile is given by

$$\rho(z) = \begin{cases} \rho_{gA} & -t_{cyl}/2 < z < t_{cyl}/2 \\ \rho_w & z \le -t_{cyl}/2 \ \ or \ \ z \ge t_{cyl}/2 \end{cases}, \qquad (S1)$$

where ρ_w is the electron density of water. To account for the smoothing effects of thermal motions, the step ED profile in Eq. S1 was convoluted with a Gaussian of 2.0 Å width to yield the final gA ED profile shown in Fig. S8. Parameters for the gA dimer are given in Table S6.

Lateral structure. The cylindrical protein domains were assumed to be randomly dispersed within the plane of a lipid bilayer vesicle. The number of domains was calculated from the total surface area of the vesicle, area per lipid, gA concentration, and the effective cross-sectional area a_{cyl} of the gA domain (Table S6). Domains were placed using a random sequential adsorption algorithm, in which trial domain centers were generated randomly and then tested against all previously placed centers for domain overlap; if any overlap existed, the trial domain center was rejected. Fig. S8 shows a representative MC snapshot of protein domains embedded in a vesicle.

Monte Carlo sampling and calculation of SAXS curves. After placing the domains within the vesicle object, random points were generated within radial segments of 0.5 Å width in both the domain and surround regions, with the number of points in a segment being proportional to the magnitude of the ED contrast of that segment with water, and the sign of each point being equal to the sign of that segment's contrast with the water (as given by the ED profiles). Typically, 2×10^3 points were generated per vesicle object. An ED contrast-weighted pair-distance distribution function $P(r)$ was then generated for the vesicle from the combined set of randomly generated points, by calculating all unique pair

distances between points of the same contrast sign (+/+ or –/–) and opposite contrast sign (+/–) and binning them into separate histograms, i.e. $P^{++}(r)$, $P^{--}(r)$, and $P^{+-}(r)$, with $P(r) = P^{++}(r) + P^{--}(r) - P^{+-}(r)$ [15]. This process was repeated for typically 2×10^4 vesicle objects with different randomly placed domains, and the $P(r)$ histograms from the individual vesicles were summed to generate an ensemble-averaged distribution $\bar{P}(r)$. The ensemble-averaged scattering intensity was then calculated as the Fourier transform of $\bar{P}(r)$ [13]:

$$\bar{I}(q) = 4\pi \int_0^\infty \bar{P}(r) \frac{\sin qr}{qr} dr. \qquad (S2)$$

S.4.3. Results

We performed three sets of simulations to isolate the effect of three variables: (1) increasing the concentration of gA transmembrane dimers in the bilayer; (2) increasing the extent of lateral gA aggregation at fixed gA concentration (protein:lipid 1:40); and (3) increasing the extent of perturbation within the first shell of lipids surrounding the gA transmembrane dimer at fixed gA concentration (protein:lipid 1:40).

Effect of increasing gA concentration. Fig. S10 reveals a dramatic liftoff at the first minimum of the simulated SAXS data (q ~ 0.28 Å^{-1}) with increasing concentration of gA transmembrane dimers. This effect arises from lateral ED contrast between the protein domain and the bilayer's hydrocarbon region at short length scales corresponding to the size of the protein domain. Excess scattering at length scales corresponding to domain sizes of tens of nanometers has been observed previously in the context of lipid phase separation in SANS experiments [14]. In that case, the lateral contrast was between an ordered (Lo) phase enriched in chain perdeuterated lipids and a disordered (Ld) phase enriched in protiated lipids [14]. A theoretical treatment of scattering from laterally heterogeneous vesicles predicts that the excess scattering intensity arising from domain/surround contrast will shift to higher q (i.e., smaller real-space distances) with decreasing domain size, and eventually migrate into the minima between scattering lobes, resulting in liftoff [13].

Effect of increasing gA lateral association. The effect of in-plane gA aggregation is shown in Fig. S11. Lateral association of gA into multimers effectively increases the domain size, which shifts the excess scattering toward lower q (i.e., larger real-space distances). The result is a *decrease* in liftoff at q ~ 0.28 Å^{-1} and an *increase* in liftoff at q ~ 0.05 Å^{-1} (far left portion of the figure) with increasing oligomerization state.

Effect of increasing bilayer perturbation. It has been reported that gA causes local thinning of the bilayer for some types of lipids [16, 17]. We investigated the effect of local perturbation by using a different ED profile corresponding to a different area per lipid for the first shell of ~ 14 lipids surrounding the gA transmembrane dimer. Fig. S12 shows the effect of the extent of this perturbation on the simulated SAXS data. Decreasing the thickness (i.e., increasing the area per lipid) of the first shell results in a slight decrease in intensity at the minimum between the first and second scattering lobes, and a slight shift of the minimum to higher q. These effects are subtler than those related to increasing gA concentration or oligomerization state, and might easily be obscured by experimental noise.

S.4.4. Conclusions

The similarity between the simulated data in Fig. S10 and the experimental SAXS data presented in the main text is striking, and strongly suggests that gA was successfully incorporated into the asymmetric vesicles. To our knowledge, ours is the first reported observation of this scattering feature in SAXS data from proteoliposomes. Moreover, because lateral association of gA showed the opposite effect in MC simulations (i.e., a rapid decrease in liftoff with increasing oligomerization, Fig. S11), gA must be predominantly unaggregated in the asymmetric vesicles. The experimental SAXS data from both symmetric and isotopically asymmetric vesicles containing gA do not show a significant change in the position of the first minimum, however conclusions about the extent of perturbation of the POPC bilayer by gA cannot be made due to the relatively poor signal-to-noise of the experimental data. Caution is also warranted due to the coarse-grained nature of the MC simulations as well as the simplifying assumptions that were used (e.g., randomly dispersed cylindrical protein domains). Finer details of the molecular shapes that are not captured by this simple model undoubtedly contribute to the coherent scattering at higher q, and indeed there is a greater discrepancy between experimental and simulated data beyond the second scattering lobe.

References:

1. Chodera, J.D., *A Simple Method for Automated Equilibration Detection in Molecular Simulations.* J Chem Theory Comput, 2016. **12**(4): p. 1799-805.
2. Doktorova, M., et al., *A new computational method for membrane compressibility: Bilayer mechanical thickness revisited.* Biophysical Journal, 2019. **116**(3): p. 487-502.
3. Johner, N., D. Harries, and G. Khelashvili, *Implementation of a methodology for determining elastic properties of lipid assemblies from molecular dynamics simulations.* BMC Bioinformatics, 2016. **17**: p. 161.
4. Johner, N., D. Harries, and G. Khelashvili, *Erratum to: Implementation of a methodology for determining elastic properties of lipid assemblies from molecular dynamics simulations.* BMC Bioinformatics, 2016. **17**(1): p. 236.
5. Doktorova, M., D. Harries, and G. Khelashvili, *Determination of bending rigidity and tilt modulus of lipid membranes from real-space fluctuation analysis of molecular dynamics simulations.* Phys Chem Chem Phys, 2017. **19**(25): p. 16806-16818.
6. Kucerka, N., M.P. Nieh, and J. Katsaras, *Fluid phase lipid areas and bilayer thicknesses of commonly used phosphatidylcholines as a function of temperature.* Biochim Biophys Acta, 2011. **1808**(11): p. 2761-71.
7. Doktorova, M., et al., *Preparation of asymmetric phospholipid vesicles for use as cell membrane models.* Nat Protoc, 2018. **13**(9): p. 2086-2101.
8. Guixa-Gonzalez, R., et al., *MEMBPLUGIN: studying membrane complexity in VMD.* Bioinformatics, 2014. **30**(10): p. 1478-80.

9. Mondal, S., et al., *Quantitative modeling of membrane deformations by multihelical membrane proteins: application to G-protein coupled receptors.* Biophys J, 2011. **101**(9): p. 2092-101.
10. Doktorova, M., et al., *Cholesterol Promotes Protein Binding by Affecting Membrane Electrostatics and Solvation Properties.* Biophys J, 2017. **113**(9): p. 2004-2015.
11. Heberle, F.A., et al., *Model-based approaches for the determination of lipid bilayer structure from small-angle neutron and X-ray scattering data.* Eur Biophys J, 2012. **41**(10): p. 875-90.
12. Kucerka, N., et al., *Structural Significance of Lipid Diversity as Studied by Small Angle Neutron and X-ray Scattering.* Membranes (Basel), 2015. **5**(3): p. 454-72.
13. Heberle, F.A., V.N. Anghel, and J. Katsaras, *Scattering from phase-separated vesicles. I. An analytical form factor for multiple static domains.* Journal of Applied Crystallography, 2015. **48**(5): p. 1391-1404.
14. Heberle, F.A., et al., *Bilayer thickness mismatch controls domain size in model membranes.* J Am Chem Soc, 2013. **135**(18): p. 6853-9.
15. Henderson, S.J., *Monte Carlo modeling of small-angle scattering data from non-interacting homogeneous and heterogeneous particles in solution.* Biophysical Journal, 1996. **70**(4): p. 1618-1627.
16. Harroun, T.A., et al., *Experimental evidence for hydrophobic matching and membrane-mediated interactions in lipid bilayers containing gramicidin.* Biophys J, 1999. **76**(2): p. 937-45.
17. Kim, T., et al., *Influence of hydrophobic mismatch on structures and dynamics of gramicidin a and lipid bilayers.* Biophys J, 2012. **102**(7): p. 1551-60.